New Journal of Physics
The open access journal at the forefront of physics

Deutsche Physikalische Gesellschaft DPG | IOP Institute of Physics

PAPER • OPEN ACCESS

Dynamics of a tracer trapped in a correlated medium in the presence of a wall

To cite this article: Marcin Piotr Pruszczyk and Andrea Gambassi 2026 *New J. Phys.* **28** 064603

IOP Publishing New J. Phys. 28 (2026) 064603 https://doi.org/10.1088/1367-2630/ae759b

New Journal of Physics
The open access journal at the forefront of physics

Deutsche Physikalische Gesellschaft DPG
IOP Institute of Physics
Published in partnership with: Deutsche Physikalische Gesellschaft and the Institute of Physics

Check for updates

OPEN ACCESS

RECEIVED
9 December 2025

REVISED
7 May 2026

ACCEPTED FOR PUBLICATION
1 June 2026

PUBLISHED
18 June 2026

PAPER

Dynamics of a tracer trapped in a correlated medium in the presence of a wall

Marcin Piotr Pruszczyk[1,2,*] and Andrea Gambassi[1,2]

[1] SISSA—International School for Advanced Studies, via Bonomea 265, 34136 Trieste, Italy
[2] INFN, via Bonomea 265, 34136 Trieste, Italy
[*] Author to whom any correspondence should be addressed.

E-mail: mpruszcz@sissa.it

Keywords: stochastic dynamics, critical Casimir forces, non-Markovian processes, correlated media

Supplementary material for this article is available online

Abstract

We describe the random motion of a particle immersed in a thermally fluctuating medium and harmonically trapped at a certain distance from a wall. The medium, modeled by a Gaussian field with a tunable correlation length ξ, is linearly coupled to the particle and evolves according to dissipative relaxational dynamics. Dirichlet boundary conditions imposed on the field at the wall give rise to a repulsive fluctuation-induced force acting on the particle, causing a shift in its average position and a renormalization of the strength of the harmonic trap. We describe the effective overdamped dynamics of the particle, which features a nonlinear memory term depending on the wall-particle separation. We show that the two-time correlation function of the particle position features a memory-induced term that depends on the distance of the particle from the wall. At the critical point, this term decays algebraically upon increasing time and it displays a crossover from the behavior observed in the bulk to that corresponding to having the particle at the wall. Our results establish a concrete connection between boundary-induced modifications of critical fluctuations and the non-equilibrium, memory-dependent dynamics of a trapped particle.

1. Introduction

The description of the random motion of mesoscopic particles in media traces back to the seminal works by Einstein [1] and Smoluchowski [2], and since then, it has remained one of the central themes of statistical physics. In a simple fluid, such motion has been successfully described in terms of a linear Langevin equation for the particle velocity v (see, e.g. [3]). In this formulation, the effective interaction between the mesoscopic colloid and the fluid molecules is modeled by a deterministic instantaneous friction $-\gamma v$ proportional to the velocity of the particle, and a random force that has a Gaussian distribution and is temporally uncorrelated. This description is valid whenever there is a clear timescale separation, i.e. if the evolution of the degrees of freedom of the medium occurs on timescales substantially shorter than those at which the motion of the particle is described.

However, when a tracer particle is immersed in a complex medium characterized by macroscopically long relaxation times, the timescale separation underlying the construction of a simple Langevin equation for particle velocity v no longer occurs and the random interaction between the particle and the medium can no longer be described by an uncorrelated Gaussian noise. Accordingly, owing to the fluctuation-dissipation theorem in equilibrium [4], the deterministic friction experienced by the particle at time t is no longer instantaneous, i.e. it does not depend solely on $v(t)$. The presence of hydrodynamic memory [5] or viscoelasticity in the medium [6, 7] provides concrete examples. In these cases, in fact, the effect of the medium on the particle dynamics is described by a retarded response $\Gamma(t)$, which determines the effective friction force as $-\int^t \mathrm{d}t'\,\Gamma(t-t')v(t')$. The kernel $\Gamma(t)$ can be experimentally inferred from studying the spectrum of the equilibrium fluctuations of the position [8] of the probe. In practice, $\Gamma(t)$ can be determined in microrheology based on the measurement of the viscoelastic shear modulus of the medium, which is related to it and which is obtained from the observation of the motion of the probe [8]. This method has been widely used in experimental investigations of the statistical properties of soft matter in recent years, see, e.g. [9–11].

The effective description of the dynamics of the probe in terms of a linear memory kernel, though applicable and accurate in many contexts, turns out to be generically insufficient for describing colloidal particles subject to optical trapping. In fact, as shown both numerically and experimentally [10, 11], the resulting memory kernel $\Gamma(t)$ turns out to depend on the details of the confinement, in particular on the trapping forces acting on the particles. This means that Γ loses the desirable feature of being determined solely by the interaction between the particle and the medium. This observation can be explained by the fact that the effective dynamics of the probe is actually governed by a nonlinear evolution equation [12]. In the simple model for which this confinement-dependent memory was derived, the medium is described by a background solvent and a fluctuating Gaussian field ϕ. This correlated field, characterized by a tunable spatial correlation length ξ, follows relaxational and locally conserved dynamics, i.e. the so-called (Gaussian) model B dynamics [13]. The motion of the colloid is described by an overdamped Langevin equation with instantaneous friction due to the interaction with the background solvent. Additionally, the probe is linearly coupled to ϕ [14–17]. Both the field ϕ and the particle are in contact with the solvent, which acts as a thermal bath. This model and its variants were employed to investigate the dynamics of particles that diffuse freely or are dragged [16, 18, 19] in the bulk or under spatial confinement [20, 21], and were successful in describing a variety of phenomena (both in and out of equilibrium) due to the presence of correlations in the medium [21–27].

The possibility of tuning the correlation length ξ and, consequently, the relaxation time of the fluctuations of the field is a property of media in the vicinity of the critical point at which they undergo a second-order phase transition. A concrete example is provided by any binary liquid mixture in the vicinity of its demixing point at which ξ diverges [28]. In these cases, however, the description of the dynamics of the media requires more refined models (see, e.g. [13, 29]) than those considered here. Due to the presence of fluctuations with long-range correlations, bodies immersed in these media (imposing boundary conditions (BCs) on such fluctuations at their surfaces) experience a fluctuation-induced force, known as the critical Casimir force [30–34], which is a thermodynamic analogue of the Casimir force observed in quantum electrodynamics [35]. Since the first theoretical prediction of the occurrence of critical Casimir forces by Fisher and de Gennes [36], these forces have been investigated theoretically in a variety of systems and within various approaches, including lattice spin systems [37, 38], quantum gases [39, 40], and field-theoretical methods [41, 42]. Moreover, they were experimentally measured, first indirectly in the film geometry [43–47], and then directly, acting on a colloidal sphere close to a flat surface [48]. These forces emerge also by confining the long-range fluctuations occurring in non-equilibrium conditions [49]. While fluctuation-induced forces have been widely investigated at equilibrium, their dynamics or occurrence out of equilibrium are still largely unexplored. In this direction, these forces have been investigated in the film geometry with fixed surfaces after a sudden temperature change [50–52], after the action of an external force [53], in granular matter [54–56], or in non-equilibrium steady states [57, 58]. The case in which the confining surfaces are allowed to move under the effect of the fluctuation-induced forces was also investigated in some instances, both theoretically [20, 21, 23, 59] and experimentally [60] in media close to a second-order phase transition.

The goal of the present study is to describe the interplay between the emergent memory in the effective dynamics of a tracer immersed in a correlated medium (see, e.g. [12]) and the fluctuation-induced force acting on the tracer. First, in section 2, we introduce the model in which the medium fills the space on one side of a $(d-1)$-dimensional flat surface (wall) at which it satisfies Dirichlet BCs. The particle is coupled linearly to the field, and it is kept away from the wall by a harmonic trap with its center at a distance X_0 from it. Both the particle and the field are in contact with an equilibrium thermal bath at temperature T. The particle evolves according to an overdamped Langevin dynamics, and the field follows relaxational dissipative dynamics [13], which satisfy the detailed balance condition. The equilibrium probability distribution function of the particle is investigated in section 3, and it is shown to feature an effective potential—representing the average effect of the fluctuation-induced force on the probe—which is repulsive and thus pushes the particle away from the wall. The effective wall-particle interaction at the critical point decays as $\sim X_1^{-(d-1)}$ with increasing wall-particle separation X_1, where d is the spatial dimensionality of the system. This behavior actually characterizes the critical Casimir force (which, strictly speaking, emerges when *all* the involved surfaces—and not solely the wall—impose BCs on the field) within the so-called small sphere approximation [61].

In the case of a one-dimensional system $d = 1$ and in the limit of a point-like particle, we describe the resulting shift of the average particle position and the suppression of thermal fluctuations quantified by its variance, due to an effective renormalization of the trap strength.

In section 4, we formulate an exact effective nonlinear and non-Markovian dynamics of the tracer, which is not invariant under spatial translations due to the presence of the wall. We show that a relation connecting the correlations of the additional field-induced noise with the effective nonlinear friction acting on the tracer ensures that the dynamics is invariant under time reversal. In section 5, we perform a perturbative expansion in the field–particle coupling constant. In $d = 1$ and in the limit of a point-like particle, we evaluate the lowest-order correction to the correlation function of the particle position. It exhibits two terms: one corresponding to the renormalization of the trap strength in the Ornstein–Uhlenbeck process, and the other stemming from memory effects present in the system. We note that, at the critical point, the latter features an algebraic behavior $\sim t^{-1/2}$ at long times t, and a crossover from an asymptotic curve characterizing the particle in the bulk to the one describing the particle trapped exactly at the wall, which is twice as large as in the bulk case. This stems from the 'propagation' of correlations in the system, similarly to what was previously reported in [23, 59]. For $d > 1$, the algebraic decay takes the form $t^{-d/2}$, and the effective 'doubling' of the memory-induced correlation occurs, due to the mirror-image construction of the BC at the wall. We also describe the power spectral density (PSD) of the process in $d = 1$, and discuss whether the presence of the wall enhances the net correlations of the particle motion, characterized by the PSD at zero frequency. In section 6, we present numerical simulations of the system in $d = 1$ dimension. We obtain the corrections to the average, the variance and the correlation function of the particle position due to the particle-field coupling, which confirm our analytical predictions. Deviations stemming from higher-order effects are also discussed. Finally, we summarize our results and formulate an outlook in section 7.

2. The model

We consider a system consisting of a tracer particle, modeling a colloid, located at position $\mathbf{X}$, and a correlated medium ϕ, with the effective Hamiltonian [22]

$$\mathcal{H}[\phi,\mathbf{X}] = \mathcal{H}_\phi[\phi] + \mathcal{H}_{\text{int}}[\phi,\mathbf{X}] + \mathcal{U}(\mathbf{X}). \tag{1}$$

The correlated medium is modeled by a fluctuating scalar field $\phi(\mathbf{x},t) \in \mathbb{R}$ characterized by the quadratic Hamiltonian [13]

$$\mathcal{H}_\phi[\phi] = \int_\Lambda \mathrm{d}^d\mathbf{x}\left[\frac{1}{2}(\nabla\phi)^2 + \frac{1}{2}r\phi^2\right]. \tag{2}$$

Here, we consider the system in a semi-infinite geometry, i.e. the field is defined for $\mathbf{x} = (x_1, x_2, \ldots, x_d) \in \Lambda = \mathbb{R}_+ \times \mathbb{R}^{d-1}$, that is, for $x_1 \geqslant 0$. Physically, this corresponds to having an impenetrable $(d-1)$-dimensional flat wall placed at $x_1 = 0$ that confines the fluctuating field to the space with $x_1 > 0$. The interaction between the field and the wall is assumed to be effectively modeled by imposing Dirichlet BCs

$$\phi(\mathbf{x})|_{x_1=0} = 0 \tag{3}$$

which suppress field modes that would otherwise have finite amplitude at the wall. In particular, long-wavelength fluctuations perpendicular to the boundary are 'reduced', since the field is constrained to vanish there. This modifies the fluctuation spectrum near the wall and, consequently, the free energy of the system. These and other BCs can be implemented directly in the effective Hamiltonian of the field by introducing the surface contribution [34]

$$\int \mathrm{d}^{d-1}\mathbf{x}_\parallel \left\{\frac{c}{2}\phi^2(x_1 = 0, \mathbf{x}_\parallel) - h\phi(x_1 = 0, \mathbf{x}_\parallel)\right\}, \tag{4}$$

where $\mathbf{x} = (x_1, \mathbf{x}_\parallel)$. Here, the surface coupling constant c is the so-called surface enhancement and h is the so-called surface field [34]. Importantly, in the absence of symmetry-breaking terms at the boundaries (i.e. for $h = 0$), and in the limit $c \to +\infty$, the Dirichlet BCs mentioned above are recovered. Moreover, these BCs emerge as the renormalization-group fixed point of the so-called ordinary transition [62, 63].

In passing, we note that in the film geometry $[0,L]\times\mathbb{R}^{d-1}$, in which the field interacts with two parallel walls placed at $x_1=0$ and $x_1=L$ via (possibly different) BCs (e.g. Dirichlet, Neumann, periodic or antiperiodic), fluctuation-mediated critical Casimir forces acting on the walls are observed [30, 33, 34, 40, 64, 65]. Importantly, the choice of BCs plays a crucial role in determining the properties of the critical Casimir forces at equilibrium [33, 34, 66]. In fact, not only does the strength of the fluctuation-induced force depend on such a choice (although the dependence is largely universal), but also its attractive or repulsive character. The parameter $r>0$ in equation (2) determines the spatial extension ξ of the correlations of the fluctuations of the field. Actually, it is related to the correlation length ξ via $\xi=r^{-\nu}$ with the critical exponent $\nu=1/2$, see [67]. In this respect, the thermally fluctuating medium can be interpreted as the order parameter of a second-order phase transition occurring at $r=0$. For instance, it can be identified with the relative concentration of the two components of a binary liquid mixture close to its demixing point.

The tracer modeling a colloidal particle [12, 17, 21–27] is described by its position $\mathbf{X}=(X_1,X_2,\dots,X_d)$ in the semi-infinite d-dimensional space Λ. It is subject to a harmonic potential

$$\mathcal{U}(\mathbf{X})=\frac{\kappa}{2}(\mathbf{X}-\mathbf{X}_0)^2 \tag{5}$$

with stiffness κ and a minimum at position $\mathbf{X}_0=\hat{\mathbf{e}}_1X_0$, where $\hat{\mathbf{e}}_1$ is the unit vector along the first spatial direction, and $X_0>0$ is the distance between the wall and the trap minimum. Additionally, the particle is coupled linearly to the field in equation (1) by

$$\mathcal{H}_{\rm int}[\phi,\mathbf{X}]=-\lambda\int_\Lambda \mathrm{d}^d\mathbf{x}\,\phi(\mathbf{x})\,V(\mathbf{x}-\mathbf{X}), \tag{6}$$

where the interaction kernel $V(\mathbf{x})$ actually models the shape of the particle and is normalized by requiring that its integral over $\mathbb{R}^d$ is one. Accordingly, the strength of the interaction between the field and the tracer is determined solely by the value of the parameter λ. In passing, we note that due to the presence of the wall at $x_1=0$, this coupling is not invariant under translations in space. This is in contrast with the cases investigated in [12, 22–27], in which the spatial integral in equation (6) was over $\mathbb{R}^d$ instead of Λ. The coupling between the field ϕ and the particle is chosen to be linear for two reasons:

(i) it breaks the $\phi\mapsto-\phi$ symmetry of the Hamiltonian of the field (2), and thus, for positive $\lambda V(\mathbf{x})$, it favors configurations of ϕ such that it is enhanced in the vicinity of the particle. When ϕ is interpreted as the order parameter of a demixing transition, the enhancement of the field around the particle models a preferential adsorption of one of the two components by the surface of the particle;

(ii) it lends itself to an exact solution of the dynamics of the field in terms of the particle coordinate $\mathbf{X}(t)$, which, in turn, enables the formulation of an exact effective dynamics of the position of the particle, as discussed further below.

It is worth mentioning that a linear coupling similar to equation (6) emerges between the bath density-fluctuation field and the position of the tracer particle when describing a tracer in a bath of dense soft colloids via the linearization of the Dean equation, see [18, 19, 68, 69]. Additionally, $V(\mathbf{x})$ is assumed to be spherically symmetric and characterized by a single lengthscale, i.e. $V(\mathbf{x})=\hat{V}(|\mathbf{x}|/R)$, where R plays the role of the effective radius of the particle. The Gaussian interaction kernel

$$V^{\rm G}(\mathbf{x})=\frac{1}{(2\pi R^2)^{d/2}}\exp\left(-\frac{\mathbf{x}^2}{2R^2}\right) \tag{7}$$

and the exponential interaction kernel

$$V^{\rm e}(\mathbf{x})=\frac{1}{2\pi^{d/2}R^d}\frac{\Gamma(d/2)}{\Gamma(d)}\exp(-|\mathbf{x}|/R) \tag{8}$$

may serve as examples. We note that in the limit $R\to0$ of a point-like particle, both $V^{\rm G}(\mathbf{x})$ and $V^{\rm e}(\mathbf{x})$ satisfy

$$V^{\rm G/e}(\mathbf{x})\xrightarrow[R\to0]{}\delta^{(d)}(\mathbf{x}). \tag{9}$$

We note that in the effective description of the interaction between the particle and the field introduced in equation (6), the field does not actually vanish in the interior of the interaction kernel $V(\mathbf{x})$, which we identify with the 'particle'. Note that after choosing the functional form of the interaction kernel, the coupling is described in terms of two effective parameters: (i) the coupling constant λ, and (ii) the effective particle radius R.

For future convenience, we recall here that the physical dimensions $[\phi]$ and $[\lambda]$ of the field and the coupling, respectively, which follow from equation (1), are given by $[\phi] = \mathcal{E}^{1/2}\mathcal{L}^{1-d/2}$ and $[\lambda] = \mathcal{E}^{1/2}\mathcal{L}^{d/2-1}$ in units of energy $\mathcal{E}$ and length $\mathcal{L}$.

2.1. Dynamics

We describe the dynamics of the position $\boldsymbol{X}$ of the particle in terms of the overdamped Langevin equation

$$\gamma_0\dot{\mathbf{X}} = -\boldsymbol{\nabla}_{\mathbf{X}}\mathcal{H} + \boldsymbol{\eta}, \tag{10}$$

where γ_0 is the drag coefficient of the tracer, and $\boldsymbol{\eta}$ is a stochastic Gaussian noise with a vanishing mean and variance given by (for simplicity, the Boltzmann constant is set to unity here and henceforth, i.e. $k_B \equiv 1$)

$$\left\langle \eta_i(t)\,\eta_j(t')\right\rangle = 2\gamma_0 T\delta_{ij}\delta(t-t'), \tag{11}$$

where T is the temperature of the equilibrium heat bath with which the particle is in contact. The evolution of the field ϕ is governed by the relaxational dynamics [29]

$$\partial_t\phi(\mathbf{x},t) = -D\frac{\delta\mathcal{H}[\phi,\mathbf{X}]}{\delta\phi(\mathbf{x},t)} + \zeta(\mathbf{x},t), \tag{12}$$

where D is the mobility of the field, and $\zeta(\mathbf{x},t)$ is the noise discussed further below. We note that equation (12) cannot be cast in the form of a continuity equation, and the field ϕ is not locally conserved. The dissipative dynamics considered here corresponds to the so-called model A, according to the classification of [13]. In the current analysis, the self-interaction term $\propto \phi^4$ present in the original formulation of this model is neglected, and we focus on its Gaussian approximation. In addition, in order to isolate the effects on the particle motion of the coupling to the fluctuating field, we neglect here the hydrodynamic degrees of freedom. Though hydrodynamic memory is known to lead to an algebraic decay of the correlation function of a Brownian particle [5, 70], its behavior is qualitatively different from the one obtained in the present study, as we discuss in more detail in section 5.2.

In previous studies [12, 22–27] in which the particle and the field were in the bulk (i.e. with $X_0 \to \infty$), the field ϕ was locally conserved in the dynamics according to the so-called model B [13]. In the bulk, this amounts to having $D \mapsto -D\nabla^2$ in equation (12), and modifying the correlations of the noise described below according to $\langle\zeta(\mathbf{x},t)\zeta(\mathbf{x}',t')\rangle \mapsto -\nabla^2\langle\zeta(\mathbf{x},t)\zeta(\mathbf{x}',t')\rangle$. In such a case, equation (12) can be cast in the form $\partial_t\phi = -\boldsymbol{\nabla}\cdot\mathbf{J}(\mathbf{x},t)$, where $\mathbf{J}$ is the corresponding current. However, in the presence of boundaries, the relationship above between the two models no longer applies. In fact, as mentioned in [21] and discussed in [52, 71], the simple Dirichlet BCs in equation (3) imposed on the field at the wall in model A are incompatible with the conserved dynamics because they lead to a non-zero flux of the field across the boundaries, which causes the field to be locally conserved away from the wall, but not globally. Technically, the issue arises due to the presence of fourth-order spatial derivatives in the equation of motion of model B. This is in contrast both with the static action and the equation of motion in the case of dissipative dynamics in which only second-order spatial derivatives are present. The BCs compatible with the local conservation of the field both in the bulk and at the boundary presented, e.g. in [71, 72] require a more elaborate treatment for constructing the corresponding Green's functions. In order to gain analytical insight into the case of Dirichlet BCs, we thus assume ϕ to follow dissipative dynamics.

Both the field and the particle are in contact with the same heat reservoir which is characterized by the temperature T. Consequently, the noise $\zeta(\mathbf{x},t)$ acting on the field $\phi(\mathbf{x},t)$ is a Gaussian variable with vanishing mean and variance

$$\langle\zeta(\mathbf{x},t)\,\zeta(\mathbf{x}',t')\rangle = 2DT\delta^{(d)}(\mathbf{x}-\mathbf{x}')\,\delta(t-t'). \tag{13}$$

Note that the correlations of the noise given by equations (11) and (13) satisfy the fluctuation-dissipation relation. As a consequence, the joint dynamics of the particle and the field is invariant under time reversal. Accordingly, the joint probability distribution function of the position of the particle and the field configuration in the resulting equilibrium steady state is given by the Boltzmann distribution $\propto \exp(-\mathcal{H}[\phi,\mathbf{X}]/T)$, where $\mathcal{H}$ is the Hamiltonian of the system introduced in equation (1).

For a system described by the Hamiltonian in equations (1), (2), (5) and (6), the equations of motion (10) and (12) read

$$\partial_t \phi(\mathbf{x}, t) = -D\left[\left(r - \nabla^2\right)\phi(\mathbf{x}, t) - \lambda V(\mathbf{x} - \mathbf{X})\right] + \zeta(\mathbf{x}, t), \tag{14}$$

$$\gamma_0 \dot{\mathbf{X}}(t) = -\kappa\left[\mathbf{X}(t) - \mathbf{X}_0\right] - \lambda \int_\Lambda \mathrm{d}^d\mathbf{x}\, \phi(\mathbf{x})\, \boldsymbol{\nabla} V(\mathbf{x} - \mathbf{X}(t)) + \boldsymbol{\eta}(t). \tag{15}$$

As in the absence of boundaries [12], these equations of motion and the imposed BC turn out to be invariant under the transformation

$$\{\phi, \lambda\} \mapsto \{-\phi, -\lambda\}, \tag{16}$$

which will prove useful in section 5.

3. Equilibrium probability distribution function

In view of the fact that the stochastic dynamics described by equations (10) and (12) with the noise terms in equations (11) and (13) satisfy the fluctuation-dissipation relation, the resulting steady state is the equilibrium one [3], and the joint probability distribution function of the particle position and the field configuration is given by the Gibbs–Boltzmann distribution

$$P(\mathbf{X}, \phi(\mathbf{x})) = \mathcal{N}^{-1} \exp\left\{-\frac{1}{T}\mathcal{H}[\phi, \mathbf{X}]\right\}, \tag{17}$$

where $\mathcal{N}$ is a normalization factor, and $\mathcal{H}[\phi, \mathbf{X}]$ is the Hamiltonian introduced in equation (1). Note that when the particle is decoupled from the field, i.e. when $\lambda = 0$, the probability density $P(\mathbf{X}, \phi(\mathbf{x}))$ factorizes. Accordingly, neglecting the possible effects that the presence of the wall may have on the particle (i.e. assuming $X_0 \to \infty$) yields a Gaussian distribution for the particle position, which is centered around $\mathbf{X_0}$ and has

$$\left[\langle X_i X_j\rangle - \langle X_i\rangle\langle X_j\rangle\right]_{\lambda=0, X_0\to\infty} = \delta_{i,j}\frac{T}{\kappa}, \tag{18}$$

where the subscript $\lambda = 0$, $X_0 \to \infty$ denotes that the averages are calculated for a particle in the bulk, decoupled from the field. This leads to a natural definition of the thermal lengthscale

$$\ell_T = \sqrt{T/\kappa}, \tag{19}$$

which describes the spatial spreading of the probability density and thus quantifies the spatial extension of the fluctuations of the position of the particle. In this work, we are primarily interested in the effects of the coupling of the particle to the fluctuating field satisfying the BCs in equation (3) and not in those occurring when the particle approaches the wall. Accordingly, henceforth, we assume that

$$X_0/\ell_T \gg 1, \tag{20}$$

$$X_0/R \gg 1, \tag{21}$$

unless stated otherwise.

When the particle and the field are coupled, i.e. for $\lambda \neq 0$, they are no longer statistically independent, and the marginal probability distribution $P(\mathbf{X})$ of the particle position $\mathbf{X}$ is obtained by integrating out the field degrees of freedom in the joint probability distribution (17), i.e. it is given by

$$P(\mathbf{X}) = \mathcal{N}^{-1} \int \mathcal{D}'\phi\, \exp\left\{-\frac{1}{T}\mathcal{H}[\phi, \mathbf{X}]\right\}, \tag{22}$$

where $\mathcal{D}'\phi$ denotes the functional integration over the configurations of the field satisfying the constraint in equation (3). The presence of the wall and the corresponding Dirichlet BCs imposed on the field $\phi(\mathbf{x})$ at $x_1 = 0$ break the spatial translational invariance of the coupling between the colloid and the medium. Accordingly, the marginal distribution $P(\mathbf{X})$ *is not* determined solely by the external harmonic trapping in equations (1) and (5) (as it occurs in the absence of the wall, see [12]), but also by the distance X_1 between the center of the probe and the wall. The resulting distribution $P(\mathbf{X})$ can be conveniently parameterized as

$$P(\mathbf{X}) = \mathcal{N}_X^{-1} \exp\left\{-\frac{1}{T}\left[\frac{\kappa(\mathbf{X}-\mathbf{X}_0)^2}{2} + V_{\text{eff}}(X_1)\right]\right\}, \tag{23}$$

where $\mathcal{N}_X$ is the normalization factor, and $V_{\text{eff}}(X_1)$ is the effective potential given by

$$V_{\text{eff}}(X_1) = -\frac{\lambda^2}{2}\int_\Lambda \mathrm{d}^d\mathbf{x}\int_\Lambda \mathrm{d}^d\mathbf{y}\, V(\mathbf{x}-\mathbf{X})\, C^D_{\phi,st}(\mathbf{x},\mathbf{y})\, V(\mathbf{y}-\mathbf{X}), \tag{24}$$

in terms of the potential V and the static (i.e. equal-time) correlation function $C^D_{\phi,st}(\mathbf{x},\mathbf{x}') = \langle\phi(\mathbf{x})\phi(\mathbf{x}')\rangle$ of the field in the presence of the wall, which satisfies Dirichlet BCs, i.e. it vanishes as $\mathbf{x}$ or $\mathbf{x}'$ approaches the wall. This correlation function can be expressed as

$$C^D_{\phi,st}(\mathbf{x},\mathbf{y}) = C_{\phi,st}(\mathbf{x}-\mathbf{y}) - C_{\phi,st}(\mathbf{x}-\mathbf{y}_R), \tag{25}$$

where $\mathbf{y}_R \equiv -y_1\hat{\boldsymbol{e}}_1 + \mathbf{y}_{||}$ is the vector obtained by reflecting $\mathbf{y} = y_1\hat{\boldsymbol{e}}_1 + \mathbf{y}_{||}$ with respect to the wall, i.e. its 'image'. In the expression above, $C_{\phi,st}(\mathbf{x})$ is the correlation function of the Gaussian field in the bulk, given by [67]

$$C_{\phi,st}(\mathbf{x}) = \int \frac{\mathrm{d}^d\mathbf{k}}{(2\pi)^d}\frac{e^{-i\mathbf{k}\cdot\mathbf{x}}}{k^2+r} = \begin{cases} \frac{\xi}{2}\mathrm{e}^{-|x|/\xi} & \text{for} \quad d=1, \\ \frac{1}{2\pi}K_0(|\mathbf{x}|/\xi) & \text{for} \quad d=2, \\ \frac{1}{4\pi|\mathbf{x}|}\mathrm{e}^{-|\mathbf{x}|/\xi} & \text{for} \quad d=3, \end{cases} \tag{26}$$

where K_0 is the modified Bessel function of the second type. The derivations of these expressions are provided in appendix A.1. Note that the expression reported in equation (23) holds for arbitrary values of the coupling λ describing the field–particle interaction (see equation (6)). Since the particle does not interact directly with the wall, the effective potential $V_{\text{eff}}(X_1)$ describes the interaction mediated by the fluctuating field. Accordingly, we call the fluctuation-induced force

$$F_{\mathrm{C}}(X_1) = -\frac{\mathrm{d}}{\mathrm{d}X_1}V_{\text{eff}}(X_1) \tag{27}$$

associated with this potential V_{eff} the Casimir-like force [34]. We note that the term *Casimir force* usually refers to the effective interaction between two bodies that impose BCs on the fluctuations of a medium [33] at their surfaces. Here, instead, the BCs in equation (3) are imposed on the field only at the wall, while the coupling between the field and the particle occurs via an interaction potential $V(\mathbf{x})$, according to equation (6). Nevertheless, the suppression of the fluctuating field at the wall in equation (3) deforms the spectrum of the fluctuations, modifying the free energy of the system, and giving rise to the Casimir-like force acting on the particle. Hence, as in a previous study [20], we refer to the force in this case as the (critical) Casimir interaction. Note also that here we focus on the average value of the fluctuation-induced force, and we do not address the issue of its fluctuations, which was discussed in a similar context in [73–75].

The force in equation (27) turns out to be repulsive, i.e. the particle is pushed away from the wall. This is somehow expected: in fact, when BCs are imposed on the field at the surfaces of both bodies, the force is generically attractive when the BCs on the two surfaces are equal but repulsive otherwise [34]. Here, the BC at the wall in equation (3) is even under $\phi \mapsto -\phi$, whereas the coupling to the particle in equation (6) is odd under such a transformation. Hence, these different symmetries of the field–wall and field–particle interaction hint towards the effective force being repulsive. Figure 1(a) presents a cartoon of the physical system in which we indicate the forces acting on the colloid. We note that, from equations (24), (26) and (27), one can show that F_{C} satisfies a scaling relation of the form

$$F_{\mathrm{C}}(X_1) = \frac{\lambda^2}{X_1^{d-1}}\Phi\left(\frac{X_1}{\xi},\frac{R}{\xi}\right), \tag{28}$$

where Φ is a dimensionless scaling function. In fact, the prefactor on the r.h.s. of this equation has the dimension of a force, i.e. $[\lambda^2/X_1^{d-1}] = \mathcal{E}/\mathcal{L}$, which follows from the discussion under equation (9). At the bulk critical point, $\xi \to \infty$ and the Casimir force exhibits an algebraic behavior as a function of the distance X_1 from the wall, with $F_{\mathrm{C}}(X_1) \sim X_1^{-(d-1)}$. When the field interacts with both bodies via BCs at their surfaces, the critical Casimir force acting on parallel planar walls separated by a distance L scales

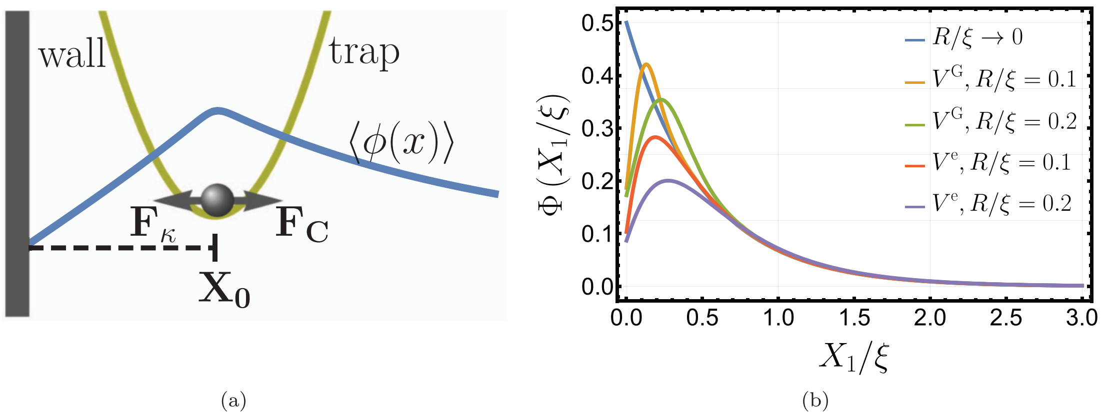

Figure 1. (a) Cartoon of the model under investigation: it comprises the tracer particle (black sphere), spatially confined by an optical trap (providing the potential represented by the dark yellow line) and interacting with a fluctuating correlated field ϕ (with the dark blue line representing its average) which vanishes at the wall according to the boundary condition (3). Due to the coupling (6) between the particle and the field, assuming λ positive (negative), it is energetically favorable for the particle to occupy the position corresponding to the maximum (minimum) of the field. Due to the Dirichlet boundary conditions (3) at the wall and the particle acting as a source of the field in equation (6), this position is farther away from the wall than the minimum of the trap at X_0. This field gives rise to a repulsive fluctuation-induced force $\mathbf{F}_\mathrm{C} = \hat{\mathbf{e}}_1 F_\mathrm{C}$ causing a shift of the particle position, counterbalanced by the force $\mathbf{F}_\kappa$ due to the trap. (b) Plot of the scaling function Φ introduced in equation (28), in the case of $d = 1$, for the Gaussian (7), the exponential (8) and the point-like (9) kernels modeling the shape of the particle, see equation (6). Note that, assuming $\xi \gg R$, the different curves coincide for $X_1/\xi \gtrsim 0.5$.

as $F_\mathrm{C} \sim L^{-d}$ at the critical point, see, e.g. [36]. If, instead of two walls, one considers a single wall and a sphere of radius R at a distance $X \gg R$ from it, the resulting fluctuation-induced force can be evaluated by means of the so-called small-sphere expansion [61, 76–78]. The resulting dependence on the distance X turns out to depend on the set of BCs considered. In particular, when the BC at at least one of the two surfaces is invariant under the transformation $\phi \mapsto -\phi$, the force scales as [76]

$$F_\mathrm{C}\,(X) \sim \frac{1}{X^{d+1-1/\nu}}, \tag{29}$$

where ν is the critical exponent introduced above equation (5). We note that in the case of the Gaussian field theory, $\nu = 1/2$ and the scaling in equation (29) yields $F_\mathrm{C}(X) \sim X^{-(d-1)}$, which is actually the same as in equation (28). Recall that in the current study, the BC (3) is invariant under the considered transformation, while the coupling (6) changes sign. Moreover, the assumptions in equations (20) and (21) and the repulsive nature of the Casimir force render $X_1/R \gg 1$. Accordingly, the case considered in this work is analogous to that described by the small-sphere expansion with at least one BC invariant under a global change of the sign of the field. In the limit $R \to 0$ of a point-like particle, the scaling functions Φ of the Casimir force take particularly simple forms

$$\Phi\left(\frac{X_1}{\xi}, 0\right) = \begin{cases} \frac{1}{2} e^{-\frac{2X_1}{\xi}} \xrightarrow[\xi\to\infty]{} \frac{1}{2}, & \text{for} \quad d = 1, \\ \frac{1}{4\pi} \frac{2X_1}{\xi} K_1\left(\frac{2X_1}{\xi}\right) \xrightarrow[\xi\to\infty]{} \frac{1}{4\pi}, & \text{for} \quad d = 2, \\ \frac{1}{16\pi} e^{-\frac{2X_1}{\xi}} \left(1 + \frac{2X_1}{\xi}\right) \xrightarrow[\xi\to\infty]{} \frac{1}{16\pi}, & \text{for} \quad d = 3, \end{cases} \tag{30}$$

where we also indicated the expressions at criticality. Note that in equation (30), the exponential decay of the force upon increasing X_1 is governed by $2X_1/\xi$. Such a dependence on *twice* the distance from the wall was also observed in previous studies on critical Casimir forces within the small sphere expansion approach [61, 76]. Here, this fact can be understood by interpreting the BC in equation (3) as being imposed by the presence of a *mirror image particle* located at the coordinate $-X_1$ along the direction orthogonal to the plane, with the coupling constant $-\lambda$. The distance between the original particle and this mirror image is then $2X_1$.

In figure 1(b), we plot the scaling function Φ defined in equation (28) for $d = 1$ and for the various forms of the interaction kernel in equation (6), i.e. for the Gaussian (7), the exponential (8), and for the point-like (9) kernel, with the corresponding expressions for $R \to 0$ reported in equation (30). We note that the different curves actually collapse onto each other for $X_1 \gtrsim \xi/2$ (recall the assumptions in equations (20) and (21)). This fact is a manifestation of the universality emerging in the system upon approaching its bulk critical point. In view of this emerging universality, the behavior of the tracer particle trapped sufficiently far from the wall can be conveniently studied by focusing on the case of the point-like potential in equation (9), as we do in what follows.

The fluctuation-induced force described above is repulsive in the sense that it pushes the particle away from the wall. Naturally, this influences the average position $\langle \mathbf{X} \rangle$ of the particle, causing its shift such that $\mathbf{F}_C$ is counterbalanced by the resulting force $\mathbf{F}_\kappa$ exerted by the trap, see figure 1(a). As it turns out, the Casimir interaction also affects its variance $\langle \mathbf{X}^2 \rangle - \langle \mathbf{X} \rangle^2$. Noting that $V_{\text{eff}}(\mathbf{x})$ is $\mathcal{O}(\lambda^2)$, one can perform a perturbative calculation in the field–particle coupling λ for the moments of the probability distribution of the particle position X_1. The derivation is presented in appendix A.2, while we report here the final expression in $d = 1$:

$$\langle X \rangle = X_0 + \frac{\lambda^2}{2\kappa} e^{-\frac{2X_0}{\xi} + \frac{2\ell_T^2}{\xi^2}} + \mathcal{O}\left(\lambda^4\right), \tag{31}$$

$$\langle X^2 \rangle - \langle X \rangle^2 = \ell_T^2 \left(1 - \frac{\lambda^2}{\kappa\xi} e^{-\frac{2X_0}{\xi} + \frac{2\ell_T^2}{\xi^2}}\right) + \mathcal{O}\left(\lambda^4\right), \tag{32}$$

where ℓ_T is the thermal length defined in equation (19). We note that the factor λ^2/κ has the dimension of a distance, see the discussion after equation (9). The presence of the Casimir force reduces the amplitude of the thermal fluctuations of the position of the colloid. In fact, $\mathbf{F}_C$ pushes the particle further away from the wall against the harmonic trap and it effectively strengthens its confinement, renormalizing the trap strength κ as

$$\kappa' = \kappa \left(1 + \frac{\lambda^2}{\kappa\xi} e^{-\frac{2X_0}{\xi} + \frac{2\ell_T^2}{\xi^2}}\right) + \mathcal{O}\left(\lambda^4\right). \tag{33}$$

Accordingly, up to terms of order λ^2, the variance in equation (32) is characterized by the renormalized thermal length $\ell_T' = \sqrt{T/\kappa'} < \ell_T$. Note that at the critical point ($\xi \to \infty$), the force given by equations (28) and (30) is constant, the average shift in the particle position (31) is maximal, equal to $\lambda^2/(2\kappa)$, while the fluctuations of the particle position (see equation (32)) are unaffected by this additional Casimir-like interaction.

We conclude by noting that a similar shift in the average position of the particle and an effective tightening of the confinement in the direction perpendicular to the wall occur for any spatial dimensionality d of the system. Moreover, in $d > 1$, the Casimir-like interaction tightens the confinement also at criticality. Indeed, neglecting thermal effects and expanding the effective potential $V_{\text{eff}}(X_1)$ around X_0, renders the potential experienced by the particle (see equation (23)) in the form

$$\begin{aligned} &\frac{\kappa}{2}(X_1 - X_0)^2 + V_{\text{eff}}(X_1) \\ &\quad \approx V_{\text{eff}}(X_0) + (X_1 - X_0) V_{\text{eff}} + \frac{1}{2}\left(\kappa + V_{\text{eff}}''(X_0)\right)(X_1 - X_0)^2 + \mathcal{O}\left((X_1 - X_0)^3\right). \end{aligned} \tag{34}$$

In $d = 1$ and for finite ξ, and for arbitrary ξ in $d > 1$, the repulsive Casimir-like force defined in equation (27) is a decreasing function of the distance, i.e. $F_C'(X_1) = -V_{\text{eff}}''(X_1) < 0$. Therefore, the effective potential has a positive curvature ($V_{\text{eff}}''(X_1) > 0$) and the renormalized trap strength $\kappa' = \kappa + V_{\text{eff}}''(X_0)$ exceeds its bare value κ. Note that in $d = 1$, equations (27), (28) and (30), in conjunction with the formula above, yield the value of κ' in agreement with equation (33) with $\ell_T = 0$.

4. Effective nonlinear dynamics of the particle

4.1. Effective dynamics

The dynamics of the Gaussian field in equation (14) is linear and, therefore, it can be integrated. The resulting expression for $\phi(\mathbf{x}, t)$ can be substituted into the equation of motion (15) of the particle, which yields the following effective non-Markovian dynamics of the tracer [12, 16, 18, 19, 22]:

$$\gamma_0 \dot{\mathbf{X}}(t) = -\kappa\left[\mathbf{X}(t) - \mathbf{X}_0\right] + \int_{-\infty}^{t} \mathrm{d}t'\, \mathbf{F}\left(\mathbf{X}(t), \mathbf{X}(t'), t - t'\right) + \boldsymbol{\Xi}\left(\mathbf{X}(t), t\right) + \boldsymbol{\eta}(t), \tag{35}$$

where the components of the emerging non-linear friction $\mathbf{F}(\mathbf{x}, \mathbf{y}, t)$ are given by

$$F_i(\mathbf{x}, \mathbf{y}, t) = -\lambda^2 \int_\Lambda \mathrm{d}^d\mathbf{x}' \int_\Lambda \mathrm{d}^d\mathbf{y}' \left[\partial_{x_i'} V(\mathbf{x}' - \mathbf{x})\right] R_\phi^D(\mathbf{x}', \mathbf{y}', t)\, V(\mathbf{y}' - \mathbf{y}). \tag{36}$$

In this expression, $R^D_\phi(\mathbf{x}',\mathbf{y}',t)$ is the response function of the Gaussian field subject to the Dirichlet BC at the wall, which vanishes whenever $\mathbf{x}'$ or $\mathbf{y}'$ belong to the boundary. In terms of the bulk response function

$$R_\phi(\mathbf{x}-\mathbf{y},t)=\int\frac{\mathrm{d}^d\mathbf{k}}{(2\pi)^d}De^{-D\left(k^2+r\right)t-i\mathbf{k}\cdot(\mathbf{x}-\mathbf{y})},\tag{37}$$

$R^D_\phi(\mathbf{x}',\mathbf{y}',t)$ in equation (36) is expressed as

$$R^D_\phi(\mathbf{x}',\mathbf{y}',t)=R_\phi(\mathbf{x}'-\mathbf{y}',t)-R_\phi(\mathbf{x}'-\mathbf{y}'_R,t),\tag{38}$$

where the reflected vector $\mathbf{y}'_R$ is defined as explained after equation (25).

Due to the presence of the wall, $\mathbf{F}(\mathbf{x},\mathbf{y},t)$ is not invariant under spatial translation, i.e. it is not a function of $\mathbf{x}-\mathbf{y}$, in contrast with the case of the system in the absence of the wall, see [12]. Additionally, the field–particle interaction induces a noise term $\boldsymbol{\Xi}(\mathbf{x},t)$ with a vanishing average and variance

$$\left\langle\Xi_i(\mathbf{x},t)\Xi_j(\mathbf{y},t')\right\rangle=TG_{ij}(\mathbf{x},\mathbf{y},|t-t'|),\tag{39}$$

where

$$G_{ij}(\mathbf{x},\mathbf{y},t)=\lambda^2\int_\Lambda\mathrm{d}^d\mathbf{x}'\int_\Lambda\mathrm{d}^d\mathbf{y}'\left[\partial_{x'_i}V(\mathbf{x}'-\mathbf{x})\right]C^D_\phi(\mathbf{x}',\mathbf{y}',t)\left[\partial_{y'_j}V(\mathbf{y}'-\mathbf{y})\right].\tag{40}$$

Here, C^D_ϕ is the correlator of the Gaussian field satisfying Dirichlet BCs

$$C^D_\phi(\mathbf{x},\mathbf{y},t)=C_\phi(\mathbf{x}-\mathbf{y},t)-C_\phi(\mathbf{x}-\mathbf{y}_R,t),\tag{41}$$

where $\mathbf{y}_R$ is the reflected vector defined after equation (25), while

$$C_\phi(\mathbf{x},t)=\int\frac{\mathrm{d}^d\mathbf{k}}{(2\pi)^d}\frac{1}{k^2+r}e^{-D\left(k^2+r\right)t-i\mathbf{k}\cdot\mathbf{x}},\tag{42}$$

is the correlator of the Gaussian field in the bulk, with $C_\phi(\mathbf{x},t=0)=C_{\phi,\mathrm{st}}(\mathbf{x})$ and thus $C^D_\phi(\mathbf{x},\mathbf{y},t=0)=C^D_{\phi,\mathrm{st}}(\mathbf{x},\mathbf{y})$, see equations (25) and (26). Moreover, we note that

$$\int_{-\infty}^t\mathrm{d}t'\,\mathbf{F}(\mathbf{x},\mathbf{x},t-t')=\hat{\boldsymbol{e}}_1F_\mathrm{C}(x_1)\equiv\mathbf{F}_\mathrm{C},\tag{43}$$

where $\mathbf{F}_\mathrm{C}$ is the Casimir-like force in equation (27), acting on the particle and directed along $\hat{\boldsymbol{e}}_1$ normal to the surface of the wall. This equality can be understood as follows: if the particle is pinned at a certain position $\mathbf{x}$, then the average force that the fluctuating field exerts on it at that position can be read from the r.h.s. of equation (35) with $\mathbf{X}(t)=\mathbf{x}$ and it is therefore given by $\int_{-\infty}^t\mathrm{d}t'\,\mathbf{F}(\mathbf{x},\mathbf{x},t-t')$, i.e. by the l.h.s. of equation (43). On the other hand, the average force exerted on a fixed particle by the field is nothing but the static fluctuation-induced force $F_\mathrm{C}(x_1)$, from which equation (43) follows immediately. Accordingly, by expressing the friction $\mathbf{F}(\mathbf{x},\mathbf{y},t)$ in equation (35) as the sum of its 'off-diagonal' component

$$\hat{\mathbf{F}}(\mathbf{x},\mathbf{y},t)\equiv\mathbf{F}(\mathbf{x},\mathbf{y},t)-\mathbf{F}(\mathbf{x},\mathbf{x},t)\tag{44}$$

and its diagonal component $\mathbf{F}(\mathbf{x},\mathbf{x},t)$ allows us to isolate the field-induced non-linear non-Markovian friction $\hat{\mathbf{F}}$ in the tracer dynamics. The resulting equation of motion of the particle then contains a term which is explicitly due to the Casimir force at equilibrium:

$$\begin{aligned}\gamma_0\dot{\mathbf{X}}(t)=&-\kappa\left[\mathbf{X}(t)-\mathbf{X}_0\right]+\mathbf{F}_\mathrm{C}(X_1(t))+\int_{-\infty}^t\mathrm{d}t'\,\hat{\mathbf{F}}(\mathbf{X}(t),\mathbf{X}(t'),t-t')\\&+\boldsymbol{\Xi}(\mathbf{X}(t),t)+\boldsymbol{\eta}(t).\end{aligned}\tag{45}$$

We note that the effective dynamics in equation (35) (or equation (45)) is exact in the sense that it describes the position of the particle for any value of the coupling constant λ of the field–particle interaction in equation (6). Notably, upon increasing the timescale separation between the dynamics of the particle and of the field—which is obtained in the *adiabatic limit* $D \to \infty$ with r finite, — $\boldsymbol{\Xi}$ and $\hat{\boldsymbol{F}}$ vanish, yielding a Markovian evolution of the position of the particle. Then, the particle-field interaction manifests itself only in the presence of the Casimir-like force, and the effective dynamics takes the form

$$\gamma_0 \dot{\mathbf{X}}(t) = -\kappa [\mathbf{X}(t) - \mathbf{X}_0] + \mathbf{F}_\mathrm{C}(X_1) + \boldsymbol{\eta}(t), \tag{46}$$

which is the Langevin equation for a particle immersed in a simple fluid interacting via fluctuation-induced forces with the wall. We refer the reader to appendix B for more details concerning the adiabatic limit.

4.2. Fluctuation-dissipation relation

The function $\mathbf{F}$ given by equation (36), describing the field-induced friction and the Casimir-like force acting on the particle, and the matrix $\mathbb{G}$ of components G_{ij} given by equation (40) and describing the correlations of the field-induced noise are related to each other via

$$-\frac{\partial}{\partial t} G_{ij}(\mathbf{x},\mathbf{y},t) = \frac{\partial}{\partial y_j} F_i(\mathbf{x},\mathbf{y},t) \quad \text{for} \quad t > 0. \tag{47}$$

As we show in appendix C, whenever this relation holds, the dynamics is invariant under time-reversal. This means that the stationary state of this process is, in fact, the equilibrium one. Accordingly, the property (47) is a manifestation of the fluctuation-dissipation relation for the nonlinear, non-translationally invariant dynamics considered in equation (35). The result above is a generalization of such a relation for translationally-invariant systems, derived in [12].

4.3. The linearized memory kernel

In order to relate the nonlinear friction $\hat{\boldsymbol{F}}(\mathbf{x},\mathbf{y},t)$ with the usual linear memory kernel, let us denote $\mathbf{X}(t) - \mathbf{X}(t') = \boldsymbol{\Delta}(t,t')$ and assume that $|\boldsymbol{\Delta}(t,t')|$ is sufficiently small to justify treating it as an expansion parameter. We use the fluctuation-dissipation relation in equation (47) to write

$$\begin{aligned}
\hat{F}_i(\mathbf{X}(t),\mathbf{X}(t'),t-t') &\simeq -\Delta_j(t,t')\,\partial_{y_j} F_i(\mathbf{x},\mathbf{y},t-t')|_{\mathbf{x}=\mathbf{y}=\mathbf{X}(t)} \\
&= \Delta_j(t,t')\,\partial_t G_{ij}(\mathbf{x},\mathbf{y},t-t')|_{\mathbf{x}=\mathbf{y}=\mathbf{X}(t)} = -\Delta_j(t,t')\frac{\mathrm{d}}{\mathrm{d}t'} G_{ij}(\mathbf{X}(t),\mathbf{X}(t),t-t'),
\end{aligned} \tag{48}$$

where we employed the Einstein summation convention. This relation allows us to rewrite the friction term in equation (45) in the form

$$\begin{aligned}
\int_{-\infty}^{t} \mathrm{d}t'\,\hat{F}_i(\mathbf{X}(t),\mathbf{X}(t'),t-t') &\approx -\int_{-\infty}^{t} \mathrm{d}t' \frac{\mathrm{d}}{\mathrm{d}t'}\left[G_{ij}(\mathbf{X}(t),\mathbf{X}(t),t-t')\right]\Delta_j(t,t') \\
&= \int_{-\infty}^{t} \mathrm{d}t'\,G_{ij}(\mathbf{X}(t),\mathbf{X}(t),t-t')\frac{\mathrm{d}}{\mathrm{d}t'}\left[\Delta_j(t,t')\right] \\
&= -\int_{-\infty}^{t} \mathrm{d}t'\,G_{ij}(\mathbf{X}(t),\mathbf{X}(t),t-t')\dot{X}_j(t'),
\end{aligned} \tag{49}$$

where the last line has the usual form of a non-Markovian (linear) friction. Moreover, it follows from equation (40) that $\mathbb{G}(\mathbf{x},\mathbf{x},t)$ depends only on the first component x_1 of $\mathbf{x}$. Accordingly, the linearization of $\mathbf{F}(\mathbf{x},\mathbf{y},t)$ in $\mathbf{x}-\mathbf{y}$ results in a linear memory kernel $\boldsymbol{\Gamma}$ (see section 1) with components Γ_{ij} which depends on the distance from the wall, given by

$$\Gamma_{ij}(x_1,t) = G_{ij}(\mathbf{x},\mathbf{x},t). \tag{50}$$

Moreover, at the lowest order in $|\mathbf{x}-\mathbf{y}|$,

$$\langle \Xi_i(\mathbf{x},t)\,\Xi_j(\mathbf{y},t')\rangle = T G_{ij}(\mathbf{x},\mathbf{y},|t-t'|) \approx T G_{ij}(\mathbf{x},\mathbf{x},|t-t'|) = T\Gamma_{ij}(x_1,t), \tag{51}$$

which is the usual fluctuation-dissipation relation for the linear stochastic dynamics [4]. Note that both the memory kernel and, consequently, the time correlation of the noise are state-dependent since they depend on X_1. Accordingly, the linearized version of the dynamics (35) features a multiplicative field-induced noise. This is in contrast with the bulk case [12], in which the linearization of the corresponding dynamics yields an additive noise term.

5. Perturbative calculation of the correlation functions

5.1. Perturbative expansion

Solving the system of equations (14) and (15) allows us to describe the dynamical behavior of the colloidal particle. However, due to the nonlinearity in $\{\phi, \mathbf{X}\}$ of the dynamics stemming from the field–particle coupling $\propto \lambda$, it is not solvable in general. Thus, we resort to a perturbative expansion in the coupling constant

$$\phi(\mathbf{x}, t) = \phi^{(0)}(\mathbf{x}, t) + \lambda\phi^{(1)}(\mathbf{x}, t) + \lambda^2\phi^{(2)}(\mathbf{x}, t) + \mathcal{O}\left(\lambda^3\right), \tag{52}$$

$$\mathbf{X}(t) = \mathbf{X}^{(0)}(t) + \lambda\mathbf{X}^{(1)}(t) + \lambda^2\mathbf{X}^{(2)}(t) + \mathcal{O}\left(\lambda^3\right). \tag{53}$$

Here, $\phi^{(0)}(\mathbf{x}, t)$ and $\mathbf{X}^{(0)}(t)$ are the solutions of equations (14) and (15) when the tracer particle and the field are decoupled, i.e. for $\lambda = 0$. In [16, 18, 19], a similar perturbative analysis was performed within the path-integral framework for the generating function of the dynamics. Here, as in [12, 22–27], we carry out a direct calculation based on the perturbative expansion of the dynamical equations. As indicated in equations (52) and (53), we will concern ourselves with the expansion up to the quadratic order in λ, as it will prove sufficient to capture the non-trivial effects on the dynamics of the tracer particle stemming from the coupling to the slow-relaxing field. We focus on the stationary properties of the system, i.e. we consider the case in which the initial conditions of the dynamics were specified at time $t_0 \to -\infty$, which renders them irrelevant. Moreover, unless stated otherwise, we shall focus below on the one-dimensional problem.

Details of the derivations of the predictions presented below are reported in appendix D. In particular, in appendix D.1, we show that perturbatively solving the equations of motion (14) and (15) renders the same steady-state average position of the particle reported in equation (31) obtained from the Gibbs–Boltzmann distribution.

5.2. Two-time correlation function

We focus here on the perturbative calculation of the connected two-time correlation function $C_c(t)$. Studying $C_c(t)$ will not only reveal the effects of the Casimir-like force on the time correlations of the process, but also how the presence of the wall affects the nonlinear memory previously derived in [12] for a particle in the bulk (i.e. for $X_0 \to \infty$).

Since the equations of motion (14) and (15) are invariant under the transformation (16), the two-time correlation function is an even function of λ, and the linear contribution vanishes:

$$C_c(t_1, t_2) = \langle X(t_1) X(t_2)\rangle - \langle X\rangle^2 = C_c^{(0)}(t_1, t_2) + \lambda^2 C_c^{(2)}(t_1, t_2) + \mathcal{O}\left(\lambda^4\right). \tag{54}$$

Regarding the validity of the perturbative approach, we note that the dimensionless parameter which controls the expansion of the correlation functions, is given by

$$g = \frac{\lambda^2}{\kappa\xi^d}, \tag{55}$$

in any dimensionality $d \geqslant 1$. This expression follows from the fact that the perturbative corrections are even functions of λ and from the discussion of the dimensionality of λ reported below equation (9). Physically, g compares the characteristic strength λ^2/ξ^d of the fluctuation-induced interaction with the stiffness κ of the harmonic trap. Accordingly, the perturbative expansion is under control for $g \ll 1$, and the λ^2 corrections remain small compared to the leading Ornstein–Uhlenbeck contribution.

For $\lambda = 0$, one recovers the Ornstein–Uhlenbeck process

$$C_c^{(0)}(t_1, t_2) = \ell_T^2 e^{-\omega_0 t} \quad \text{with} \quad t = |t_1 - t_2|, \tag{56}$$

where ℓ_T is the thermal lengthscale defined in equation (19), and $\omega_0 = \kappa/\gamma_0$ is the relaxation rate of the colloid in the harmonic trap. The details of the calculation of $\lambda^2 C_c^{(2)}(t)$ are presented in appendix D.2, while here we report the final expression

$$\lambda^2 C_c^{(2)}(t) = \lambda^2 C_{c,\mathrm{C}}^{(2)}(t) + \lambda^2 C_{c,\mathrm{memo}}^{(2)}(t), \tag{57}$$

where

$$\lambda^2 C_{c,\mathrm{C}}^{(2)}(t) = -\frac{\lambda^2 \ell_T^2}{\kappa\xi} e^{-\frac{2X_0}{\xi} + \frac{2\ell_T^2}{\xi^2}} e^{-\omega_0 t}(1 + \omega_0 t) \tag{58}$$

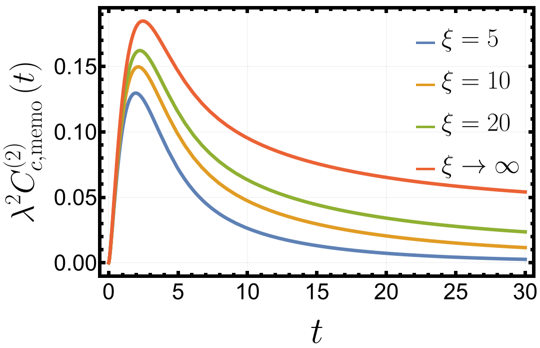

(a)

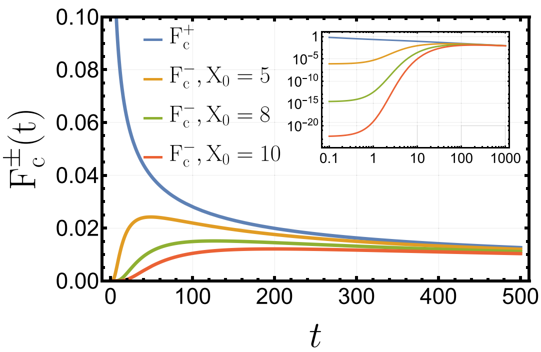

(b)

Figure 2. (a) Memory-induced contribution $\lambda^2 C^{(2)}_{c,\mathrm{memo}}(t)$ to the correlation function in equation (59) as a function of time t for $X_0 = 10$. Note that this contribution vanishes at $t = 0$ since it takes a finite amount of time for the memory to 'build up'. After an initial growth $\sim t^{3/2}$ stemming from the $\sim t^{-1/2}$ behavior of the memory (65) integrated in equation (59), $\lambda^2 C^{(2)}_{c,\mathrm{memo}}(t)$ attains its maximal value at $t \approx 2$ and then, upon further increasing t, it decreases either exponentially for finite ξ, or algebraically $\sim t^{-1/2}$ for $\xi \to \infty$. (b) Bulk (F^+) and wall (F^-) critical contributions to the memory given by equations (63) and (64), respectively, as functions of time t. We note that F^+ and F^- coincide at long times. In the inset, we plot $F^{\pm}$ on a log–log scale in order emphasize the different order of magnitudes of the bulk and the wall contributions at short times. Quantities in this figure are plotted for $\lambda^2/(2\kappa) = \ell_T = \sqrt{D/\omega_0} = 1$.

is the Casimir contribution and

$$\lambda^2 C^{(2)}_{c,\mathrm{memo}}(t) = \frac{\lambda^2 \ell_T^2}{\kappa \xi} \int_0^{\omega_0 t} \mathrm{d}u\, (\omega_0 t - u)\, e^{-(\omega_0 t - u)} \mathcal{F}(u) \tag{59}$$

is the memory-induced contribution to the two-point function. In the equation above, $\mathcal{F}$ denotes the emergent dimensionless memory

$$\begin{aligned} \mathcal{F}(u) = &\int \frac{\mathrm{d}\nu}{2\pi} \frac{\nu^2}{1+\nu^2} e^{-\left(D/\omega_0 \xi^2\right) u \left(1+\nu^2\right)} e^{-(\ell_T/\xi)^2 \nu^2 \left(1 - e^{-u}\right)} \\ &+ \int \frac{\mathrm{d}\nu}{2\pi} \frac{\nu^2}{1+\nu^2} e^{-\left(D/\omega_0 \xi^2\right) u \left(1+\nu^2\right)} e^{-(\ell_T/\xi)^2 \nu^2 \left(1 + e^{-u}\right)} \cos\left(2\left(X_0/\xi\right)\nu\right), \end{aligned} \tag{60}$$

with the closed-form expressions obtained after the integration reported in section D.2, cf, equations (137), (145), (146), (153), (154) and (156). The function $\mathcal{F}(u)$ defined above is proportional to $\langle G\left(X^{(0)}(t+u), X^{(0)}(t), u\right)\rangle$ with $u > 0$, where G is given by equation (40) (we omit here the indication of the indices of G, since we consider the case $d = 1$, where they take only one value), and $\langle \cdot \rangle$ denotes averaging over the stationary Ornstein–Uhlenbeck process. We note that at $t = 0$, the memory-induced contribution (59) vanishes, and the Casimir contribution (58) reduces to the expression reported in equation (32). Moreover, the Casimir contribution is independent of the diffusion coefficient D and, therefore, it is not affected by taking the adiabatic limit (see the discussion above equation (46)), whereas the memory term depends on D and vanishes in this limit (see appendix B and equation (137) for details). Finally, it follows from equations (56) and (58) that renormalizing the relaxation rate according to $\omega_0 \mapsto \omega_0' = \kappa'/\gamma_0$ with κ' defined in equation (33), renders

$$C^{(0)}_c(t) + \lambda^2 C^{(2)}_{c,\mathrm{C}}(t) = \ell_T'^2 e^{-\omega_0' t} + \mathcal{O}\left(\lambda^4\right), \tag{61}$$

where ℓ_T' was introduced after equation (33). We recognize equation (61) as the two-time correlator of the Ornstein–Uhlenbeck process with the renormalized trap strength. In figure 2(a), we present a plot of $\lambda^2 C^{(2)}_{c,\mathrm{memo}}(t)$ for various values of ξ in the case of $\lambda^2/(2\kappa) = \ell_T = \sqrt{D/\omega_0} = 1$ and $X_0 = 10$. At criticality ($r = 0$), its long-time behavior is characterized by an algebraic decay $\propto t^{-1/2}$. For finite values of r, it decays exponentially at long times. We note that both $C^{(0)}_c(t)$ and $\lambda^2 C^{(2)}_{c,\mathrm{C}}(t)$ decay exponentially upon increasing time, irrespective of the value of the parameter r. Accordingly, at the critical point, the memory-induced term is the dominant one at long times.

Interestingly, the memory-induced term $\lambda^2 C^{(2)}_{c,\mathrm{memo}}(t)$ depends on X_0, and the emergent memory $\mathcal{F}$ in equation (59) can be decomposed into two terms

$$\mathcal{F}(u) = \mathcal{F}^{+}(u) + \mathcal{F}^{-}(u), \tag{62}$$

where $\mathcal{F}^{+}$ does not depend on the wall-trap separation X_0, whereas $\mathcal{F}^{-}$ does, and it vanishes in the bulk, i.e. in the limit $X_0 \to \infty$. We refer to them as the bulk and the wall contributions to the dimensionless memory, respectively. The expressions of $\mathcal{F}^{+}$ and $\mathcal{F}^{-}$ for $r > 0$ are provided by the first and the second term in equation (60), respectively. The integration over ν therein renders rather lengthy closed-form expressions reported in equations (153), (154) and (156). Here, we focus on the simpler expressions obtained at the critical point $r = 0$:

$$\frac{1}{\xi}\mathcal{F}^{+}(\omega_0 t) \xrightarrow[\xi\to\infty]{} \frac{1}{\sqrt{4\pi\left[Dt + \ell_T^2\left(1 - e^{-\omega_0 t}\right)\right]}} = F_c^{+}(t), \tag{63}$$

$$\frac{1}{\xi}\mathcal{F}^{-}(\omega_0 t) \xrightarrow[\xi\to\infty]{} \frac{\exp\left[-\frac{X_0^2}{Dt+\ell_T^2(1+e^{-\omega_0 t})}\right]}{\sqrt{4\pi\left[Dt + \ell_T^2\left(1 + e^{-\omega_0 t}\right)\right]}} = F_c^{-}(t), \tag{64}$$

where ℓ_T is the thermal length defined in equation (19), and we denote by $F_c^{\pm}(t)$ the critical contributions to the memory. (Note that in taking the limit $\xi \to \infty$ in the equations above, we have accounted for the fact that $\lambda^2 C^{(2)}_{c,\mathrm{memo}}(t)$ in equation (59) depends on $\mathcal{F}^{\pm}$ via $\mathcal{F}/\xi$, owing the prefactor $\propto 1/\xi$ of the integral.) The plots of $F_c^{\pm}(t)$ are presented in figure 2(b). In the inset, the quantities are plotted on a log–log scale, which highlights the different magnitudes of the wall and the bulk contributions at short times. To understand the physical significance of both contributions, we investigate their asymptotic behavior. In particular, for the bulk contribution, we find

$$F_c^{+}(t) \approx \begin{cases} \frac{1}{\sqrt{4\pi[D+(T/\gamma_0)]t}}, & \text{for} \quad \omega_0 t \ll 1, \\ \frac{1}{\sqrt{4\pi\left(Dt+\ell_T^2\right)}}, & \text{for} \quad \omega_0 t \gg 1, \end{cases} \tag{65}$$

while, for the wall contribution,

$$F_c^{-}(t) \approx \begin{cases} \frac{1}{2\sqrt{2\pi\ell_T^2}}\exp\left[-\frac{X_0^2}{2\ell_T^2}\right], & \text{for} \quad \omega_0 t \ll 1, \\ \frac{1}{\sqrt{4\pi\left(Dt+\ell_T^2\right)}}\exp\left[-\frac{X_0^2}{Dt+\ell_T^2}\right], & \text{for} \quad \omega_0 t \gg 1. \end{cases} \tag{66}$$

Note that, within the short-time regime $t \ll \omega_0^{-1}$, $F_c^{+}(t)$ displays an integrable singularity $\propto t^{-1/2}$ (recall that $F_c^{+}(t)$ determines the integrand in equation (59)), giving rise to the initial $t^{3/2}$ growth of the memory-induced contribution to the two-point function, while $F_c^{-}(t)$ approaches a constant value which, due to the assumption (20), is very small. Moreover, at times $t \gtrsim t^* = (X_0^2 - \ell_T^2)/D \approx X_0^2/D$, the wall contribution becomes comparable with the bulk contribution (see the argument of the exponent in equation (66)), and they coincide as $t \to \infty$. The physical interpretation of these observations is as follows: at short times, the position of the particle is strongly correlated with its initial position (testified by the $t^{-1/2}$ singularity of the memory as $t \to 0$), and the colloid is not significantly affected by the presence of the wall due to the assumption in equation (20). However, because of the presence of long-range correlations at criticality, the field disturbed by the random motion of the particle is correlated with the field in the vicinity of the wall. The time required for these correlations to propagate is of the order of magnitude of the typical diffusion time across the distance X_0 with diffusivity D. A similar effect of 'retardation' of fluctuation-induced forces was discussed in [23, 59, 79]. Finally, at very long times, the wall contribution coincides with the bulk contribution. This is because, as we discussed below equation (30), the imposition of the BC (3) at the wall can be interpreted as a consequence of the presence of a mirror-image particle at $-X$ coupled to the field with coupling $-\lambda$. At long times, the correlations due to this second 'virtual' particle are observed.

The behavior of the memory discussed above affects the memory-induced contribution to the correlation function in equation (59). In figure 3(a), we plot $\lambda^2 C^{(2)}_{c,\mathrm{memo}}(t)$ on a log–log scale for $r = 0$ and various values of the distance X_0 between the minimum of the trap and the wall. For concreteness, we consider $\lambda^2/(2\kappa) = \ell_T = \sqrt{D/\omega_0} = 1$. For comparison, we plot two asymptotic curves: one corresponding to the limit $X_0 \to \infty$, i.e. the asymptotic bulk behavior, and one corresponding to $X_0 = 0$, which we call the wall asymptotic. Note that the latter, for $t \gg \omega_0^{-1}$, turns out to be twice as large as the curve corresponding to the case $X_0 \to \infty$, which stems from the correlations with the mirror-image particle at $-X$.

For finite distances from the wall, at short times, $\lambda^2 C^{(2)}_{c,\mathrm{memo}}(t)$ follows the bulk asymptotic behavior; at moderate times, it crosses over to the wall asymptotic, which it follows at longer times. Note that as the wall-particle separation increases, the crossover time also increases, in agreement with equation (66).

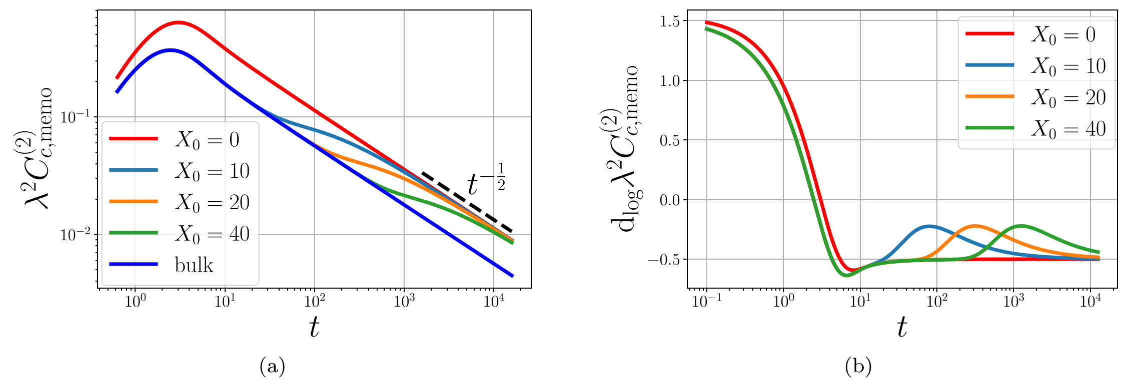

Figure 3. Memory-induced contribution $\lambda^2 C^{(2)}_{c,\mathrm{memo}}(t)$ to the correlation function in equation (59) at the critical point $r = 0$ and as a function of time t. (a) Plot on a log–log scale of $\lambda^2 C^{(2)}_{c,\mathrm{memo}}(t)$, which highlights the algebraic decay $\propto t^{-1/2}$ at long times. Additionally to the plots obtained for finite values of X_0, we present the asymptotic curves corresponding to $X_0 = 0$ (upper curve) and $X_0 \to \infty$ (lower curve). For finite values of X_0, one observes a crossover from the bulk asymptotic to the wall asymptotic. (b) Logarithmic derivative (see equation (67)) of $\lambda^2 C^{(2)}_{c,\mathrm{memo}}(t)$ as a function of time t. At short times, the values of the logarithmic derivative approaches $3/2$, corresponding to a $\propto t^{3/2}$ growth of the memory-induced contribution, whereas it takes the value $-1/2$ at long times, corresponding to the algebraic behavior discussed above. The bumps in the plots indicate the times at which the crossovers from the bulk to the wall asymptotic occur. Note that the larger X_0, the longer the crossover time. Both plots correspond to $\lambda^2/(2\kappa) = \ell_T = \sqrt{D/\omega_0} = 1$.

To highlight the crossover of $\lambda^2 C_{c,\mathrm{memo}}(t)$ from wall asymptotic to bulk asymptotic, we consider its logarithmic derivative $\mathrm{d}_{\log}$, which, for a (positive) function $f(t)$ is defined as

$$\mathrm{d}_{\log} f(t) = \frac{\mathrm{d}\log f(t)}{\mathrm{d}\log t}. \tag{67}$$

This logarithmic derivative quantifies the 'local' algebraic decay of the function $f(t)$. The plot of $\mathrm{d}_{\log}\lambda^2 C_{c,\mathrm{memo}}(t)$ is provided in figure 3(b). For X_0 finite, the curves exhibit a bump indicating the crossover, with the bumps occurring at increasingly longer times upon increasing X_0. At long times, the asymptotic value $-1/2$ of the logarithmic derivative corresponds to the algebraic decay presented in figure 3(a); at short times, instead, the derivative takes the value $3/2$ which can be inferred from equation (59) in conjunction with equation (65). This corresponds to the initial rapid growth of $\lambda^2 C^{(2)}_{c,\mathrm{memo}}(t)$ observed in figure 2(a).

We note that for $d > 1$ and in the absence of the wall ($X_0 \to \infty$), the correction to the particle correlation function at the critical point is characterized by a long-time ($\omega_0 t \gg 1$) algebraic tail of the form

$$\lambda^2 C^{(2)}_c(t) \sim \ell_T^2 \frac{\lambda^2}{\kappa} (4\pi D t)^{-d/2}. \tag{68}$$

The derivation is given in appendix F. The algebraic law $\sim t^{-d/2}$ differs from that obtained for model B dynamics [12], where it is $\sim t^{-d/4}$. This difference follows directly from the dynamical critical exponent: the typical timescale τ_ϕ scales with the correlation length as $\tau_\phi \sim \xi^z$, with $z = 2$ for model A and $z = 4$ for model B.

We note that for $d > 1$, the Casimir correction in equation (58) to the particle two-point function, which arises from the renormalization of the trap strength in equation (34), persists and, crucially, does not vanish at the critical point. This is in contrast with the one-dimensional case discussed under equation (34). Furthermore, at any $d \geqslant 1$, at the critical point and for times $t \gg X_0^2/D$, the wall contribution to the memory asymptotically equals the bulk contribution. This follows from the construction of the Dirichlet BCs (3) by the method of images, as described below equation (66). Consequently, the long-time algebraic tail of the memory-induced correction to the particle correlation function is asymptotically twice the bulk result—as shown for $d = 1$ in figure 3(a).

We note here that, in $d = 3$, the bulk critical memory-induced contribution to the correlator in equation (68) is characterized by an algebraic decay governed by the same exponent as the correlation $C_{\mathrm{Hd}}(t)$ of the particle position due to hydrodynamic memory [5]

$$C_{\mathrm{Hd}}(t) \sim -\ell_T^2 \frac{\gamma_0}{\kappa} t^{-3/2} \sqrt{\frac{R^2 \rho_f}{4\pi \eta_f}}, \tag{69}$$

where R is the radius of the spherical particle, ρ_f is the density of the fluid in which the particle is immersed, and η_f its shear viscosity. Crucially, this $C_{\mathrm{Hd}}(t)$ describes an anticorrelation of the particle motion, whereas the coupling of the particle to the slow-relaxing field leads to its additional correlation. Again, we note that in the case of conservative dynamics, the fluctuation-induced memory decays $\sim t^{-d/4}$ (see [12]), and consequently dominates the hydrodynamic term at long times. Moreover, the presence of the wall enhances the fluctuation-induced memory (see equation (62)) without changing the exponent governing the algebraic decay in time, while it reduces the memory effects due to hydrodynamics, decreasing the exponent of the decay, as demonstrated for the velocity autocorrelation function in [70].

5.3. Power spectral density

In the context of the experimental analysis of the dynamics of tracer particles in fluid media, it is natural to consider the power spectral density (PSD) $S(\omega)$ [80] of the particle position $X(t)$, which is defined as the Fourier transform
of $C_c(t)$:

$$S(\omega) = \int \mathrm{d}t\, C_c(t)\, e^{i\omega t} = S^{(0)}(\omega) + \lambda^2 S^{(2)}(\omega) + \mathcal{O}(\lambda^4). \tag{70}$$

In the decoupled case $\lambda = 0$, the zeroth-order term $S^{(0)}(\omega)$ corresponds to the PSD of the Ornstein–Uhlenbeck process

$$S^{(0)}(\omega) = \frac{\ell_T^2}{\omega_0} \frac{2\omega_0^2}{\omega_0^2 + \omega^2}, \tag{71}$$

while the second-order term is given by

$$\lambda^2 S^{(2)}(\omega) = \lambda^2 S^{(2)}_{\mathrm{C}}(\omega) + \lambda^2 S^{(2)}_{\mathrm{memo}}(\omega); \tag{72}$$

in this expression we distinguish, as done in section 5.2, the Casimir contribution

$$\lambda^2 S^{(2)}_{\mathrm{C}}(\omega) = -\frac{\lambda^2 \ell_T^2}{\kappa\omega_0\xi} \frac{4\omega_0^4}{\left(\omega_0^2+\omega^2\right)^2} e^{-\frac{2X_0}{\xi} + \frac{2\ell_T^2}{\xi^2}} \tag{73}$$

from the memory-induced contribution

$$\lambda^2 S^{(2)}_{\mathrm{memo}}(\omega) = \frac{\lambda^2 \ell_T^2}{\kappa\omega_0\xi} \frac{2\omega_0^4}{\left(\omega_0^2+\omega^2\right)^2} \int_0^\infty \mathrm{d}u\, \mathcal{F}(u) \left[\cos\left(\frac{u\omega}{\omega_0}\right)\left(1 - \frac{\omega^2}{\omega_0^2}\right) - 2\sin\left(\frac{u\omega}{\omega_0}\right)\frac{\omega}{\omega_0}\right] \tag{74}$$

to the PSD, which is expressed in terms of $\mathcal{F}(u)$, given by equation (60). The details of the derivation of these expressions are provided in appendix E. Similarly to the case of the two-time correlator in equation (61), we rewrite the contribution to the PSD which is independent of the memory as

$$S^{(0)}(\omega) + \lambda^2 S^{(0)}_{\mathrm{C}}(\omega) = \frac{\ell_T'^2}{\omega_0'} \frac{2\omega_0'^2}{\omega_0'^2 + \omega^2} + \mathcal{O}(\lambda^4). \tag{75}$$

This equation expresses the PSD of the Ornstein–Uhlenbeck process with the renormalized trap strength κ' given by equation (33), which renormalizes both the thermal lengthscale ℓ_T' and the relaxation rate ω_0', introduced after equation (33) and before equation (61), respectively. In order to investigate the properties of the memory-induced contribution to the PSD in equation (74), we express it as

$$\lambda^2 S^{(2)}_{\mathrm{memo}}(\omega) = \lambda^2 S^{(2)}_{\mathrm{memo},+}(\omega) + \lambda^2 S^{(2)}_{\mathrm{memo},-}(\omega), \tag{76}$$

which follows from introducing in equation (74) the decomposition of $\mathcal{F}(u)$ as the sum of the bulk term $\mathcal{F}^+(u)$ and the wall term $\mathcal{F}^-(u)$ according to equation (62). It turns out that at the critical point $r = 0$, both $\lambda^2 S^{(2)}_{\mathrm{memo},+}(\omega)$ and $\lambda^2 S^{(2)}_{\mathrm{memo},-}(\omega)$ develop a singularity $\propto \omega^{-1/2}$ at small $\omega \to 0$. This asymptotic behavior is observed also for small but finite values of ω in the case of large but finite values of ξ (i.e. for $r \neq 0$), as indicated by a dashed line in figure 4(a), in which the bulk term $\lambda^2 S^{(2)}_{\mathrm{memo},+}(\omega)$ of the memory-induced contribution to the PSD is plotted for $\lambda^2/(2\kappa) = \ell_T = \sqrt{D/\omega_0} = 1$. To gain more insight into the behavior of $\lambda^2 S^{(2)}_{\mathrm{memo},\pm}$, we report here their expressions at the critical point and at the lowest order in ℓ_T (corresponding to the limit of strong confinement $\ell_T \to 0$), i.e. considering

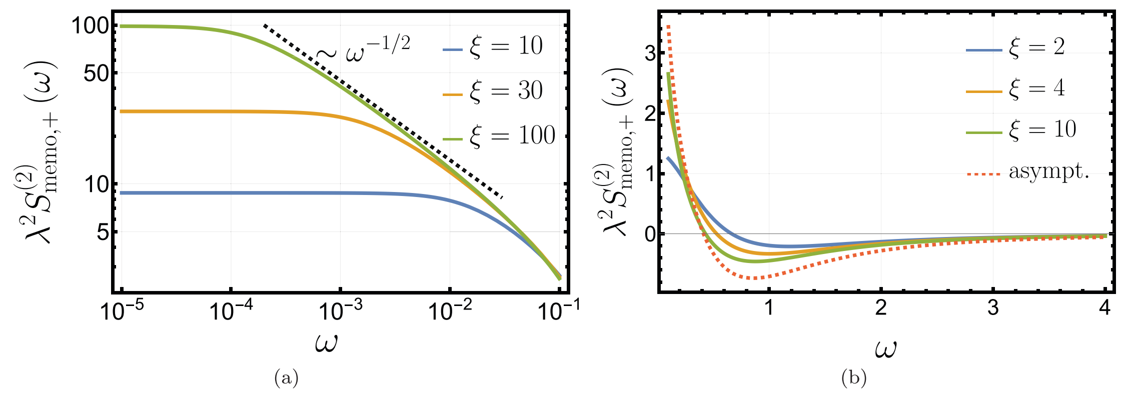

Figure 4. The bulk term of the memory-induced contribution $\lambda^2 S^{(2)}_{\mathrm{memo},+}(\omega)$ to the power spectral density as a function of ω, for various values of the correlation length ξ. (a) For large values of ξ, one observes $\lambda^2 S^{(2)}_{\mathrm{memo},+}(\omega) \propto \omega^{-1/2}$ (dotted line) at small but finite values of ω. (b) At larger values of ω, instead, $\lambda^2 S^{(2)}_{\mathrm{memo},+}(\omega)$ shows a non-monotonic behavior and, in fact, after becoming negative, it approaches zero from below as $\omega \to \infty$. The various curves are compared with the one obtained at the critical point for strong confinement, see equation (77) (dashed line). The solid lines in both panels were obtained with $\lambda^2/(2\kappa) = \ell_T = \sqrt{D/\omega_0} = 1$.

only the dependence on ℓ_T of the prefactor ℓ_T^2. In this limit, the bulk term of the memory-induced contribution is

$$\lambda^2 S^{(2)}_{\mathrm{memo},+}(\omega) = \frac{\lambda^2 \ell_T^2}{2\kappa\omega_0}\sqrt{\frac{2\omega_0}{D}}\frac{\omega_0^4}{(\omega_0^2+\omega^2)^2}\left(\frac{\omega}{\omega_0}\right)^{-1/2}\left[1 - 2\left(\frac{\omega}{\omega_0}\right) - \left(\frac{\omega}{\omega_0}\right)^2\right], \tag{77}$$

and the wall term is

$$\lambda^2 S^{(2)}_{\mathrm{memo},-}(\omega) = \frac{\lambda^2 \ell_T^2}{2\kappa\omega_0}\sqrt{\frac{2\omega_0}{D}}\frac{\omega_0^4}{(\omega_0^2+\omega^2)^2}\left(\frac{\omega}{\omega_0}\right)^{-1/2}\sqrt{2}e^{-\sqrt{\frac{2\omega}{D}}X_0} \times\left\{\left[1 - \left(\frac{\omega}{\omega_0}\right)^2\right]\cos\left(\frac{\pi}{4} + \sqrt{\frac{2\omega}{D}}X_0\right) - 2\left(\frac{\omega}{\omega_0}\right)\sin\left(\frac{\pi}{4} + \sqrt{\frac{2\omega}{D}}X_0\right)\right\}. \tag{78}$$

Recall that the wall term is due to a mirror-image particle located at position $-X$. We note that equations (77) and (78) coincide at $X_0 = 0$ because then the positions of the particle and its mirror image are the same. Moreover, they exhibit the same behavior at small ω, i.e. the prefactors of the singularity $\propto \omega^{-1/2}$ are the same in both cases, irrespective of the value of X_0. This corresponds to the fact that, at long times, the presence of the wall doubles the correlation of the particle position, which corresponds to the crossover of the correlation function presented in Figure 3(a). Finally, we note that the wall term $\lambda^2 S^{(2)}_{\mathrm{memo},-}(\omega)$ in equation (78) vanishes, upon increasing ω, more rapidly than the bulk term $\lambda^2 S^{(2)}_{\mathrm{memo},+}(\omega)$ in equation (77), with an exponential decay $\propto \exp(-\sqrt{2\omega/D}X_0)$ instead of the algebraic one observed in equation (77). We recall that, at short times, the correlations due to the presence of the wall are extremely small, see equation (66), which explains the large-ω behavior of the PSD discussed above.

We note that, from the definition of the PSD in equation (70), it follows that

$$\int \frac{\mathrm{d}\omega}{2\pi} S(\omega) = C_c(0). \tag{79}$$

It can be shown by a direct calculation that the Casimir contribution to the PSD given by equation (73) satisfies

$$\int \frac{\mathrm{d}\omega}{2\pi}\lambda^2 S_{\mathrm{C}}(\omega) = \lambda^2 C_c^{(2)}(0), \tag{80}$$

with $\lambda^2 C_c^{(2)}(0)$ given by equations (57) and (58), which implies, together with equation (79), that the integral over ω of the memory-induced contribution $\lambda^2 S^{(2)}_{\mathrm{memo}}(\omega)$ to the PSD in equation (74) vanishes. This is actually expected, because it follows from the fact that the equal-time correlation of the

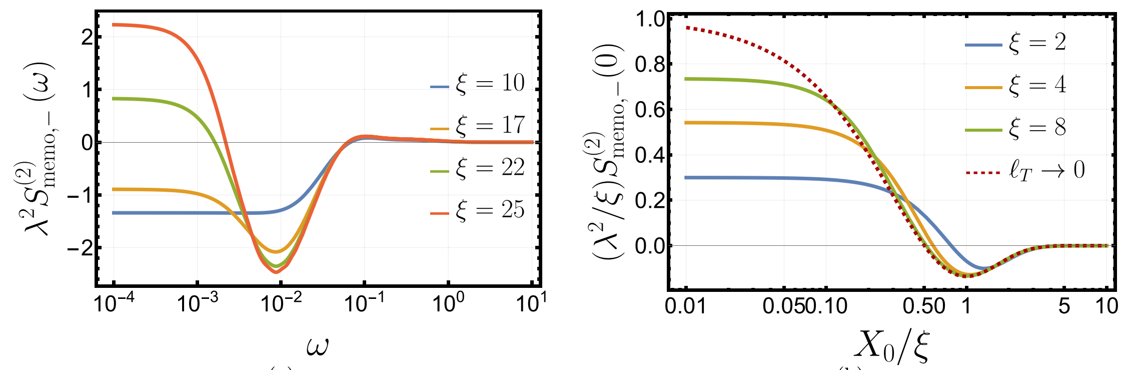

Figure 5. The wall term of the memory-induced contribution $\lambda^2 S^{(2)}_{\mathrm{memo},-}(\omega)$ to the power spectral density for various values of the correlation length ξ, as a function of (a) ω with fixed $X_0 = 10$ or (b) X_0 with $\omega = 0$. Note that $\lambda^2 S^{(2)}_{\mathrm{memo},-}(\omega)$ is generically a non-monotonic function of its variables and, for a fixed value of X_0, it attains a finite value for $\omega \to 0$, the sign of which depends on ξ, see panel (a). The dashed line in panel (b) corresponds to $(\lambda^2/\xi) S^{(2)}_{\mathrm{memo},-}(\omega = 0)$ in the limit of strong confinement, given by equation (83), which changes sign at $X_0/\xi = 0.5$ and attains its minimal value at $X_0/\xi = 1$. The solid lines in both panels are plotted for $\lambda^2/(2\kappa) = \ell_T = \sqrt{D/\omega_0} = 1$.

particle position in the steady state is the equilibrium one, in which only the Casimir force $\mathbf{F}_{\mathrm{C}}$ appears. Moreover, since this holds for any value of X_0, the wall and the bulk terms have to independently satisfy

$$\int \frac{d\omega}{2\pi} \lambda^2 S^{(2)}_{\mathrm{memo},\pm}(\omega) = 0, \tag{81}$$

as one can verify in the limit of strong confinement by a direct integration of equations (77) and (78). Equation (81) implies that $\lambda^2 S^{(2)}_{\mathrm{memo},\pm}(\omega)$ is a non-monotonic function of ω, which takes both positive and negative values. This non-monotonic behavior is clearly visible in figures 4(b) and 5(a), in which $\lambda^2 S_{\mathrm{memo},+}(\omega)$ and $\lambda^2 S_{\mathrm{memo},-}(\omega)$ are plotted, respectively. Finally, we investigate the behavior of $\lambda^2 S^{(2)}_{\mathrm{memo},\pm}(\omega)$ at $\omega = 0$, which is given by

$$\lambda^2 S^{(2)}_{\mathrm{memo},\pm}(\omega = 0) = \frac{2\lambda^2 \ell_T^2}{\kappa \omega_0 \xi} \int_0^\infty du \, \mathcal{F}^\pm(u). \tag{82}$$

It quantifies the net effect of the bulk and wall terms on the correlations of the particle position. For a finite correlation length ξ, $\lambda^2 S^{(2)}_{\mathrm{memo},+}(\omega = 0)$ has a finite positive value which grows linearly upon increasing ξ. As observed in figure 5(a), the wall term $\lambda^2 S^{(2)}_{\mathrm{memo},-}(\omega = 0)$ may take both negative and positive values at $\omega = 0$. To further examine this, we note that, in the limit of strong confinement $\ell_T \to 0$,

$$\lambda^2 S^{(2)}_{\mathrm{memo},-}(\omega = 0) = \frac{\lambda^2 \ell_T^2}{2\kappa} \frac{\xi}{D} \left(1 - \frac{2X_0}{\xi}\right) e^{-\frac{2X_0}{\xi}}. \tag{83}$$

Hence, in this limit, it is positive for $\xi > 2X_0$ and negative for $\xi < 2X_0$. Additionally, we plot $(\lambda^2/\xi) S^{(2)}_{\mathrm{memo},-}(0)$ in figure 5(b) for $X_0 = 10$ and $\lambda^2/(2\kappa) = \ell_T = \sqrt{D/\omega_0} = 1$ together with the asymptotic curve given by equation (83) indicated by a dashed line. The physical interpretation of equation (83) and figure 5(b) is the following: in the limit of strong confinement, at the lowest order in λ, the particle localized at $X \simeq X_0$ affects the field in its vicinity. Such a perturbed portion of the medium is correlated over the distance given by the correlation length ξ. For $2X_0 < \xi$, the correlations of the particle increase due to the presence of the wall (with positive $\lambda^2 S_{\mathrm{memo},-}(0)$), which stems from the effective interaction with the *mirror image particle* trapped at $-X_0$. For $2X_0 > \xi$, the particle and its mirror image are uncorrelated. The only effect of the presence of the wall is that the field does not fill the entire space and there is less medium that could 'store' the memory about the previous motion of the particle. Hence, the memory-induced correlations are suppressed and $\lambda^2 S_{\mathrm{memo},-}(0)$ is negative. Taking into account the thermal effects, the particle is effectively delocalized according to a Gaussian distribution and is spread over a typical distance given by ℓ_T defined in equation (19), and the plots in figure 5(b) flatten. Finally, we note that, independently of the value of X_0/ξ, the presence of the memory enhances correlations of the particle position, i.e. $\lambda^2 S^{(2)}_{\mathrm{memo}}(0) = \lambda^2 S^{(2)}_{\mathrm{memo},+}(0) + \lambda^2 S^{(2)}_{\mathrm{memo},-}(0)$ is always positive.

6. Numerical simulations

In this section, we verify numerically the accuracy of the perturbative expansion based on equations (52), (53) and (55). In particular, we consider the case of $d = 1$ in the stationary state and focus on the shift of the average particle position due to the field–particle coupling λ, i.e.

$$\langle \Delta X \rangle = \langle X \rangle - \langle X \rangle|_{\lambda=0}, \tag{84}$$

and on the correction

$$\Delta C_c(t) = C_c(t+t_0, t_0) - C_c(t+t_0, t_0)|_{\lambda=0}, \tag{85}$$

to the connected correlation function $C_c(t_1, t_2)$ (see equation (54)), where the subtracted quantities in the equations above refer to the case of the absence of coupling between the particle and the field. First, we investigate the static properties by plotting the numerically obtained $\langle \Delta X \rangle$ in equation (84) and the variance given by $\Delta C_c(t=0)$ in equation (85), as functions of λ. We compare the numerical data with the corresponding perturbative predictions reported in equations (31) and (32), respectively. Subsequently, for fixed $\lambda = 0.25$, we determine numerically the correction to the correlation function in equation (85) as a function of time t, and compare it with the expressions in equations (57)–(59), derived within the perturbative expansion.

In the simulation, we approximate the semi-infinite geometry $\Lambda = \mathbb{R}_+$ by a box of size L, and impose Dirichlet BCs on the fluctuating field at both boundaries, i.e. we fix $\phi(0,t) = \phi(L,t) = 0$. This allows us to expand $\phi(x,t)$ as

$$\phi(x,t) = \sqrt{\frac{2}{L}} \sum_{n=1}^{n_{\max}} a_n(t) \sin(k_n x), \quad \text{with} \quad k_n = \frac{n\pi}{L}, \tag{86}$$

where the amplitudes $a_n(t)$ are independent stochastic variables. In the limit $L \to \infty$, the mode sum converges to the continuum result, and all physical quantities reported are independent of L, provided that it is sufficiently large. Also, we approximate the kernel describing the point-like limit in equation (9) by the Gaussian in equation (7) with an effective radius R, which gives each mode n an effective coupling damped by the factor $e^{-k_n^2 R^2/2}$. Note that finite-R corrections enter at order $\mathcal{O}(k^2 R^2)$ and are negligible for $kR \ll 1$.

We performed Langevin dynamics simulations of the equations of motion (14) and (15), in which the particle position $X(t)$ and the field modes $\{a_n\}$ were propagated simultaneously using a first-order Euler–Maruyama scheme [81]. We chose the time-step $\Delta t = 5 \times 10^{-4}$, and the field modes were updated via exact Ornstein–Uhlenbeck integration at each step. Each simulation comprised 2×10^6 steps, and the first 5×10^5 and 10^6 steps were discarded before determining the position mean and variance, respectively. Additionally, physical quantities were measured every 20 steps in order to reduce correlations. The shift of the average position (84) and of the variance (85) were estimated using multiple paired independent seeds—each seed running both a $\lambda = 0$ and a $\lambda \neq 0$ trajectory from the same initial noise sequence—which substantially reduces the variance of the estimator. Statistical uncertainties are reported as the standard error of the mean across seeds.

For simulations of both quantities, we chose $\kappa = \gamma_0 = 1$. In order to optimize the signal-to-noise ratio, for $\langle \Delta X \rangle$, which we plot against λ^2 in figure 6(a), we chose $T = 0.1$, $X_0 = 8$, $r = 0.0025$, $D = 10$, $L = 250$, $R = 0.5$. The simulation updated $n_{\text{modes}} \approx 955$ field modes, which corresponds to $k_{\max} R = 6$. The statistics were obtained for 20 independent seeds of the noise, which rendered a small statistical error. The data were obtained for a set of λ's corresponding to $g \in [0, 0.2]$, see equation (55). We notice that for $\lambda \leqslant 0.8$ ($g \leqslant 0.032$), the relative error between the average obtained in the simulation and the perturbative expansion is below 2%, and the theoretical predictions remain within the error bars. As λ increases, so does the relative error, reaching up to 8% for $\lambda = 2$. This discrepancy stems from higher-order effects captured by the simulation.

In the case of the variance, with the corresponding plot presented in figure 6(b), the simulation turned out to be more sensitive to finite-size effects. Accordingly, the corresponding data were obtained for $L = 1000$ with $k_{\max} R = 3$, giving $n_{\max} \approx 9550$ modes. We set $T = 1$ and $r = 0.04$ (notice the T-dependence in ℓ_T^2 and $1/\xi$ in the prefactor in equation (32)), and chose $D = 5$, $R = 0.1$, and $X_0 = 4$. The statistics were obtained for 200 independent seeds of the noise. The set of λ's considered here correspond to $g \in [0, 0.05]$, see equation (55). Due to thermal noise, the uncertainty is substantially larger than above, with the relative standard error remaining above 10% across the full range of parameters

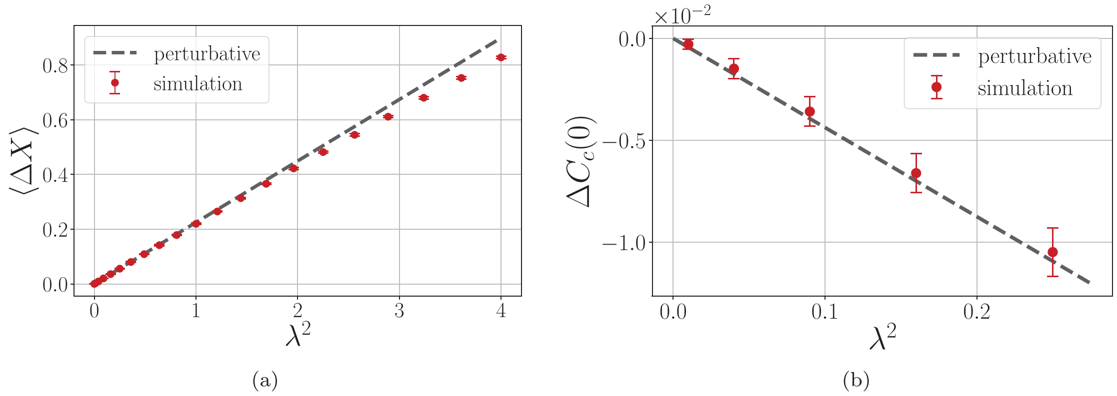

Figure 6. (a) Average shift of the particle position $X(t)$ obtained from numerical simulations (symbols). For $\lambda \lesssim 0.8$, corresponding to $g \lesssim 0.032$ (see equation (55)), the theoretical prediction derived within the perturbative expansions in equation (31) (dashed line) agrees with the results of the simulations with a relative error below 2%, and the theoretical predictions remain within the error bars. Upon increasing λ, the expansion predicts a larger value than the simulation, as a consequence of neglecting higher order terms. (b) Shift in the variance of the particle position $X(t)$ obtained from numerical simulations (symbols), compared with the theoretical prediction in equation (32) (dashed line), derived within perturbation theory. For the values of λ explored here, i.e. $\lambda \lesssim 0.5$ ($g \lesssim 0.05$), the numerical data agree with the theoretical predictions (consistently with what is observed in panel (a)), within the statistical uncertainties.

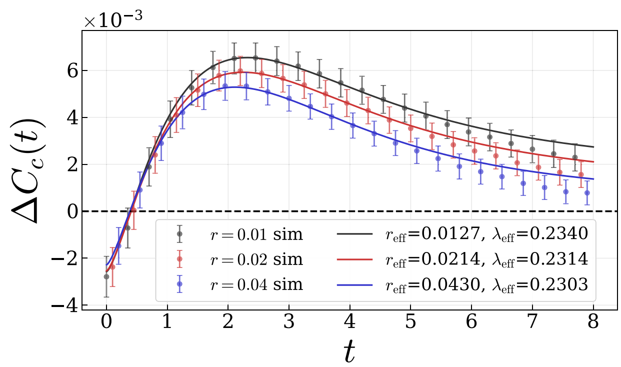

Figure 7. Correction to the two-point function $\Delta C_c(t)$, given in equation (85) (symbols with errorbars) evaluated numerically for $\lambda = 0.25$, $X_0 = 4$, and various values (indicated by different colors) of the distance r from the critical point. The corresponding solid lines indicate the analytical prediction given by equations (57)–(59), where the values of the coupling constant λ and the parameter r were fitted to the data up to $t_{\rm max} = 5$.

explored. We conclude that the data are consistent with the theoretical prediction, but that the present simulations are not able to resolve deviations at the level of the expected corrections.

Figure 7 shows the numerical determination of the corrections $\Delta C_c(t)$ defined in equation (85) (symbols with errorbars) to the time-dependent correlation function $C_c(t)$ of the particle stemming from its coupling to the field, plotted as a function of time t. In the simulations we set $\lambda = 0.25$, $T = D = 1$, $R = 0.1$, $r \in \{0.01, 0.02, 0.04\}$ (corresponding to different colors), $X_0 = 4$ and $L = 1000$ with $k_{\rm max} R = 3$, giving $n_{\rm max} \approx 9{,}550$ modes. The data were collected from 300 statistically independent runs. These corrections exhibit (i) negative values at short times, stemming from the renormalization of the trap strength due to the Casimir interaction; (ii) a slow decay upon increasing t, demonstrating the presence of memory in the system. For comparison, in figure 7 we report the analytical prediction given by equations (57)–(59) (solid lines), where the values of the coupling constant λ and the deviation r from criticality were determined by fitting to the data up to $t_{\rm max} = 5$. The fit hints towards an effective weakening of the coupling $\lambda = 0.25 \mapsto \lambda_{\rm eff} \approx 0.232$ and a shift away from criticality $r \mapsto r_{\rm eff} > r$, both stemming from higher-order effects, not captured in the lowest-order perturbative calculation. Up to this renormalization of the parameters, the perturbative prediction turns out to capture qualitatively and, to some extent quantitatively, the behavior of the numerical data.

7. Conclusions

We presented an analytical study of the equilibrium properties and of the effective dynamics of a tracer particle in a solvent, linearly coupled to a fluctuating Gaussian field with relaxational dissipative dynamics and subject to harmonic trapping. The field has a tunable correlation length ξ, is subject to Dirichlet BCs at the surface of a planar wall at a distance X_0 from the minimum of the trap, and fills the space only on one side of the wall. Both the particle and the field are in contact with a thermal bath with temperature T. In the present study, we assume X_0 to be much larger than the (effective) size of the particle and the typical lengthscale ℓ_T of the thermal fluctuations of the particle position inside the trap.

First, we derived the equilibrium distribution of the position $\mathbf{X}$ of the colloidal particle. We showed that, in addition to the harmonic potential of the optical trap, the Gibbs–Boltzmann probability distribution of $\mathbf{X}$ features an effective potential describing the interaction between the wall and the particle, mediated by the fluctuating field. The resulting fluctuation-induced force, which we called the Casimir-like force (due to its similarity to the forces acting on bodies imposing BCs on fluctuations on their surfaces), turned out to be repulsive, i.e. it pushes the particle away from the wall. We introduced a scaling function for this force in equation (28), and showed that in the limit of a small particle and at the critical point $\xi \to \infty$, the value of the force scales $\sim X_1^{-(d-1)}$ upon increasing its distance X_1 from the wall, where d is the dimensionality of the system. We demonstrated that, in the lowest quadratic order in λ, in $d = 1$, and in the limit of a point-like particle, the Casimir-like force not only shifts the average position of the particle $\langle X \rangle$, but also influences the variance $\langle X^2 \rangle - \langle X \rangle^2$ by renormalizing the strength of the optical trap, see equation (33), such that the thermal fluctuations of the particle position are actually reduced. These results were verified numerically in section 6. At the critical point, the shift of the average position $\langle X \rangle$ is maximal, whereas the effects on the variance vanish.

We presented the effective dynamics of the particle in equation (45), which is expressed by a nonlinear non-Markovian Langevin equation featuring the force due to the trap, the fluctuation-induced force, a non-instantaneous friction, and an additional field-induced noise term. The friction, which is not invariant under spatial translations, turned out to be related to the correlations of the field-induced noise via the extended fluctuation-dissipation relation reported in equation (47), which we proved to ensure the invariance of the dynamics under time reversal. We discussed the adiabatic limit of the dynamics, i.e. the limit $D \to \infty$ of the mobility D of the field, with ξ finite, in which the dynamics becomes Markovian, and the only effect of the coupling of the particle to the field is the emergence of the Casimir-like force. Finally, we noted that the linearization of the effective dynamics of the particle features a multiplicative noise term and a linear memory kernel satisfying the usual fluctuation-dissipation relation [4].

Having discussed the properties of the exact effective dynamics of the tracer, we performed a perturbative calculation in the field–particle interaction for the connected two-time correlation function $C_c(t) = \langle X(t)X(0) \rangle - \langle X \rangle^2$ of the colloid position X, expanding in powers of the coupling constant λ. For simplicity, we focused on the one-dimensional case $d = 1$, assuming a point-like particle. The lowest-order correction, quadratic in λ, featured two terms: (i) a Casimir term $\lambda^2 C^{(2)}_{c,\mathrm{C}}(t)$ which renders the change of the variance of the particle position at $t = 0$. The sum of this term and the correlator obtained in the decoupled case ($\lambda = 0$) renders the two-point function of the Ornstein–Uhlenbeck process with the renormalized trapping strength mentioned above; (ii) a memory-induced term $\lambda^2 C_{c,\mathrm{memo}}(t)$ which vanishes for $t = 0$. We expressed the latter in terms of the dimensionless memory $\mathcal{F}$, see equation (59), and demonstrated its dependence on the distance between the center of the optical trap and the wall in the case of the system at criticality. In particular, at short times, the effects due to the presence of the wall are negligible, whereas at longer times, the presence of the wall doubles the memory-induced correlations because of an effective interaction with a *mirror image particle* at position $-X$.

We discussed the behavior of $\lambda^2 C_{c,\mathrm{memo}}(t)$ which, for finite values of X_0, displays a crossover from the asymptotic behavior corresponding to the bulk $X_0 \to \infty$ case, featuring a decay $\sim t^{-1/2}$ at long times, to that corresponding to the trap placed exactly at the wall, characterized by the same power-law, but with a prefactor twice as large as in the bulk. Based on the mirror-image construction, we generalized this result to $d > 1$ with the algebraic scaling taking the form $t^{-d/2}$. We also discussed the properties of the power spectral density (PSD), i.e. the Fourier transform of the two-time correlation of the particle position, focusing in particular on the non-monotonic behavior of the memory-induced contribution to the PSD. Finally, we showed that the presence of the wall might enhance or diminish the correlations of the particle position, depending on the distance of the particle from the wall, on the value of the correlation length, and on the spatial extent of thermal fluctuations of the particle position, quantified by the PSD at zero frequency.

The results presented above motivate further investigations of the behavior of tracer particles in correlated media in the presence of a wall. In fact, several open questions remain, including the impact of different forms of coupling between the field, the wall, and the particle—such as symmetry-breaking BCs at the wall or a quadratic coupling to the particle—that may lead to attractive fluctuation-induced forces. Future work should also consider the role of the self-interaction for the field (e.g. $\propto \phi^4$) and possible hydrodynamic effects in the particle and the field dynamics. In fact, they are key elements of more realistic models of the dynamics of near-critical media. Additionally, the regime in which the particle remains confined near the wall—which requires accounting for direct wall-particle interactions—warrants additional study. Finally, the present analysis can be extended to non-equilibrium settings, including scenarios where the particle is dragged by a trap moving at constant velocity, oscillating at a fixed frequency, or in active-matter systems in the presence of a wall.

Acknowledgment

We thank Sarah A M Loos, Marco Baiesi, Aljaz Godec and Davide Venturelli for constructive discussions.

Data availability statement

All data that support the findings of this study are included within the article (and any supplementary files).

Supplementary data 1 available at https://doi.org/10.1088/1367-2630/ae759b/data1.
Supplementary data 2 available at https://doi.org/10.1088/1367-2630/ae759b/data2.
Supplementary data 3 available at https://doi.org/10.1088/1367-2630/ae759b/data3.
Supplementary data 4 available at https://doi.org/10.1088/1367-2630/ae759b/data4.
Supplementary data 5 available at https://doi.org/10.1088/1367-2630/ae759b/data5.
Supplementary data 6 available at https://doi.org/10.1088/1367-2630/ae759b/data6.

Appendix A. Equilibrium distribution

In this appendix, we sketch the calculations yielding the equilibrium properties of the system. In particular, in appendix A.1, the expression of the marginal equilibrium distribution of the particle position in equation (23) and the corresponding effective potential (24) are derived. In appendix A.2, we turn our attention to the case of $d = 1$ with a point-like particle (9), and sketch the perturbative calculation of the lowest-order correction in λ to $\langle X\rangle$ and $\langle X^2\rangle - \langle X\rangle^2$, reported in equations (31) and (32) respectively.

A.1. Effective potential

In equilibrium, the probability distribution describing the position $\mathbf{X}$ of the colloidal particle is given by the marginal of the Gibbs–Boltzmann distribution in equation (22). To trace out the field degrees of freedom therein, i.e. to perform the functional integration, we express the field-dependent part of the Hamiltonian in equations (2) and (6) in a bilinear form

$$\mathcal{H}_\phi[\phi] + \mathcal{H}_{\rm int}[\phi,\mathbf{X}] = \int_\Lambda \mathrm{d}^d\mathbf{x} \int_\Lambda \mathrm{d}^d\mathbf{x}' \left\{\frac{1}{2}\phi(\mathbf{x})\hat{A}(\mathbf{x},\mathbf{x}')\phi(\mathbf{x})\right\} - \lambda \int_\Lambda \mathrm{d}^d\mathbf{x}\,\phi(\mathbf{x})\,V(\mathbf{x}-\mathbf{X}), \tag{87}$$

with $\hat{A}(\mathbf{x},\mathbf{x}') = \delta^{(d)}(\mathbf{x}-\mathbf{x}')(r-\nabla^2)$ and $\Lambda = \mathbb{R}_+ \times \mathbb{R}^{d-1}$. The functional integration in equation (22) is Gaussian, and hence, it can be evaluated

$$\int \mathcal{D}'\phi\, e^{-[\mathcal{H}_\phi[\phi]+\mathcal{H}_{\rm int}[\phi,\mathbf{X}]]/T} \propto \exp\left[\frac{\lambda^2}{2T}\int_\Lambda \mathrm{d}^d\mathbf{x}\int_\Lambda \mathrm{d}^d\mathbf{x}'\,V(\mathbf{x}-\mathbf{X})\,\hat{A}^{-1}(\mathbf{x},\mathbf{x}')\,V(\mathbf{x}'-\mathbf{X})\right], \tag{88}$$

where $\hat{A}^{-1}$ is the inverse operator of $\hat{A}$. These operators are not translationally invariant since they are defined on the space of fields vanishing at $x_1 = 0$. To determine $\hat{A}^{-1}(\mathbf{x},\mathbf{x}')$, we express the field in the basis of combinations of plane waves vanishing at the wall, i.e. we write

$$\phi(\mathbf{x}) = \int_\Lambda \frac{\mathrm{d}^d\mathbf{k}}{(2\pi)^d}\,\phi_{\mathbf{k}}\,2\sin(k_1x_1)\,e^{-i\mathbf{k}_\parallel\cdot\mathbf{x}_\parallel}, \tag{89}$$

which satisfies

$$\phi_{\mathbf{k}} = \int_{\Lambda} \mathrm{d}^d\mathbf{x}\, \phi(\mathbf{x})\, 2\sin(k_1 x_1)\, e^{i\mathbf{k}_{\parallel}\cdot\mathbf{x}_{\parallel}}. \tag{90}$$

Then, one can cast the operator $\hat{\boldsymbol{A}}(\mathbf{x},\mathbf{x}')$ in this basis

$$\tilde{\boldsymbol{A}}(\mathbf{k},\mathbf{k}') = \left(r+k^2\right)(2\pi)^d\,\delta(k_1-k_1')\,\delta^{(d-1)}\left(\mathbf{k}_{\parallel}+\mathbf{k}_{\parallel}'\right), \tag{91}$$

whose inverse is given by

$$\tilde{\boldsymbol{A}}^{-1}(\mathbf{k},\mathbf{k}') = \frac{1}{r+k^2}(2\pi)^d\,\delta(k_1-k_1')\,\delta^{(d-1)}\left(\mathbf{k}_{\parallel}+\mathbf{k}_{\parallel}'\right). \tag{92}$$

Using the expansion in plane waves in equation (89), we obtain

$$\hat{\boldsymbol{A}}^{-1}(\mathbf{x},\mathbf{x}') = \int \frac{\mathrm{d}^d\mathbf{k}}{(2\pi)^d}\frac{1}{r+k^2}\left[e^{-i\mathbf{k}\cdot(\mathbf{x}-\mathbf{x}')} - e^{-i\mathbf{k}\cdot(\mathbf{x}-\mathbf{x}'_R)}\right] \equiv C^D_{\phi,\mathrm{st}}(\mathbf{x},\mathbf{x}'), \tag{93}$$

with $C^D_{\phi,\mathrm{st}}(\mathbf{x},\mathbf{x}')$ introduced in equation (24). Performing the above integration yields the results reported in equations (23), (24) and (26).

A.2. Equilibrium perturbative calculation for the 1-point and 2-point functions

In this appendix, we consider the case of the point-like particle in equation (9) in one spatial dimension $d=1$. We briefly describe the calculation of the lowest-order correction in λ to the average and the variance of the position of this particle, which are reported in equations (31) and (32), respectively. Since $V_{\mathrm{eff}}(X_1)$ is $\mathcal{O}(\lambda^2)$, expanding the exponent in equation (23) in powers of λ yields

$$\exp\left\{-\frac{\kappa(\mathbf{X}-\mathbf{X}_0)^2}{2T} - \frac{V_{\mathrm{eff}}(X_1)}{T}\right\} = e^{-\frac{\kappa(\mathrm{x}-\mathrm{x}_0)^2}{2T}}\left(1-\frac{V_{\mathrm{eff}}(X_1)}{T}\right) + \mathcal{O}\left(\lambda^4\right). \tag{94}$$

For the delta-like particle-field interactions considered here, the translationally invariant part of the static correlation function $C^D_{\phi,st}(\mathbf{x},\mathbf{x}')$, i.e. the part which is a function of $(\mathbf{x}-\mathbf{x}')$ in equations (24)–(26) is irrelevant, as it renders an X_1-independent constant. Hence, one can focus on

$$\tilde{V}_{\mathrm{eff}}(X_1) = \frac{\lambda^2}{2}C_{\phi,\mathrm{st}}(2X_1). \tag{95}$$

Assuming (20), integration over $\Lambda=\mathbb{R}_+$ can be approximated by the integration over $\mathbb{R}$. In addition, the same assumption allows us to approximate the argument $|2X_1|/\xi$ of the exponential in the effective potential (see equation (26)) by $2X_1/\xi$, since the contribution from $X_1<0$ will be negligibly small. Accordingly, these approximations render the relevant integrals Gaussian, and a straightforward calculation for the normalization constant $\mathcal{N}_X$ in equation (23) within this perturbative approach -leads to

$$\mathcal{N}_X = \sqrt{2\pi}\,\ell_T\left(1-\frac{\lambda^2\xi}{4T}e^{-\frac{2X_0}{\xi}+\frac{2\ell_T^2}{\xi^2}}\right) + \mathcal{O}\left(\lambda^4\right). \tag{96}$$

From this, averages of X and X^2 are obtained from straightforward Gaussian integrals over $\mathbb{R}$, which are reported in equations (31) and (32), respectively.

Appendix B. Adiabatic approximation

In this appendix, we elaborate on the concept of the *adiabatic limit*, in which the effective dynamics of the colloid in equation (35) becomes Markovian. For convenience, let us consider the case $d=1$. The approximation of instantaneous equilibration of the medium formally corresponds to taking the limit $D\to\infty$ while keeping r (equivalently ξ) finite. It can be shown that, for a D-independent function $f(t)$,

$$\int_{-\infty}^{t}\mathrm{d}t'\,R^D_{\phi}(x,y,t-t')f(t') \xrightarrow[D\to\infty]{} \frac{\xi}{2}\left[e^{-\frac{|x-y|}{\xi}} - e^{-\frac{|x+y|}{\xi}}\right]f(t), \tag{97}$$

where R_ϕ^D is the response function satisfying the Dirichlet BCs at the wall, introduced in equations (37) and (38). From the property above, it follows that

$$\int_{-\infty}^{t} \mathrm{d}t' \, \frac{1}{D} R_\phi^D(x,y,t-t') f(t') \xrightarrow[D\to\infty]{} 0. \tag{98}$$

Accordingly, from Eqs (24), (26), (27) and (97), the function F introduced in the effective dynamics (35) and given by equation (36) (here we drop the vectorial notation, given that the force $\mathbf{F}$ has only one component F in $d=1$) satisfies

$$\int_{-\infty}^{t} \mathrm{d}t' F(X(t), X(t'), t-t') \xrightarrow[D\to\infty]{} F_\mathrm{C}(X(t)), \tag{99}$$

where F_C is the Casimir-like force defined in equation (27). Moreover, the field-induced noise Ξ introduced in equation (35) is given by

$$\Xi(x,t) = -\lambda \int_0^\infty \mathrm{d}z \int_0^\infty \mathrm{d}z' \, V'(z-x) \int_{-\infty}^{t} \mathrm{d}t' \, \frac{1}{D} R_\phi^D(z,z',t-t') \xi(z',t') \tag{100}$$

and, according to equation (98), satisfies

$$\Xi(X(t),t) \xrightarrow[D\to\infty]{} 0, \tag{101}$$

where Ξ indicates the only component of $\boldsymbol{\Xi}$ in $d=1$. An analogous argument holds in higher spatial dimensionality $d>1$. Accordingly, in the adiabatic approximation, the effective dynamics is Markovian and given by equation (46).

Appendix C. Time reversal symmetry

In this appendix, we show that the effective dynamics in equation (35) with the noise term $\boldsymbol{\eta}$ satisfying equation (11), the field-induced noise $\boldsymbol{\Xi}$, characterized by the variance (39) and expressed in terms of the matrix elements of $\mathbb{G}$, and the nonlinear force $\boldsymbol{F}$ is indeed invariant under time-reversal, provided that the latter two satisfy the relation in equation (47). A similar argument was presented in [12] in the case of the particle in the bulk. The argument will be provided for the case of $d=1$, but it readily generalizes to higher dimensions. For clarity of presentation, we omit the vectorial notation, understanding that in $d=1$ all quantities under investigation are scalar.

We start by noticing that equation (47) makes it convenient to introduce a function $\psi(x,y,t)$ given by

$$\psi(x,y,t) = \int_t^\infty \mathrm{d}t' \, F(x,y,t'), \tag{102}$$

which satisfies

$$F(x,y,t) = -\partial_t \psi(x,y,t), \tag{103}$$
$$G(x,y,t) = \partial_y \psi(x,y,t). \tag{104}$$

Moreover, we note that

$$F_\mathrm{C}(x) = -\frac{\mathrm{d}}{\mathrm{d}x} V_\mathrm{eff}(x) = \int_{-\infty}^{t} \mathrm{d}t' \, F(x,x,t-t') = \psi(x,x,0). \tag{105}$$

Additionally, the following symmetries of $G(x,y,t)$ will prove useful in what follows:

$$G(x,y,t) = G(x,y,|t|), \tag{106}$$
$$G(y,x,t) = G(x,y,t). \tag{107}$$

In order to investigate the possible time-reversal symmetry of the dynamics, we introduce its path-integral representation in terms of the Martin–Siggia–Rose [82–84] action

$$S[x(t),p(t)] = S_0[x(t),p(t)] + S_\mathrm{int}[x(t),p(t)],$$

where S_0 is the action without the field (Ornstein–Uhlenbeck process with $\lambda = 0$) and S_{int} is the term stemming from the particle-field interaction. The former is given by

$$S_0[x(t), p(t)] = \frac{\kappa(x_{-\infty} - X_0)^2}{2T} - i\int dt\, p(t)[\gamma_0 \dot{x}(t) + \kappa(x(t) - X_0)] + \gamma_0 T \int dt\, p^2(t), \tag{108}$$

where $x_{-\infty} = x(t \to -\infty)$ is the initial condition drawn from the Gibbs–Boltzmann distribution, and $p(t)$ is the so-called response field. As demonstrated in [16], S_{int} is given by

$$\begin{aligned} S_{\text{int}}[x(t), p(t)] = \frac{V_{\text{eff}}(x_{-\infty})}{T} + i\int dt dt'\, \theta(t - t') p(t) F(x(t), x(t'), t - t') \\ + \frac{T}{2}\int dt dt'\, p(t) G(x(t), x(t'), t - t') p(t'). \end{aligned} \tag{109}$$

We can now use the method presented in [85] to show that the relations (103) and (104) accompanied by equation (105) guarantee time-reversal symmetry of the stationary process described by the considered dynamics, i.e. that it is an equilibrium process. For a given trajectory $\{x(t), p(t)\}$, its time-reversed counterpart $\{\bar{x}(t), \bar{p}(t)\}$ is given by [85]

$$x(t) \mapsto \bar{x}(t) = x(-t), \tag{110}$$

$$p(t) \mapsto \bar{p}(t) = p(-t) - \frac{i}{T}\dot{x}(-t), \tag{111}$$

where the dot above a function denotes the derivative with respect to the argument. In the case of equilibrium processes, the corresponding action satisfies $S[x,p] = S[\bar{x},\bar{p}]$ which is the property that we prove now. It can be easily shown that $S_0[\bar{x},\bar{p}] = S_0[x,p]$. The proof of the fact that $S_{\text{int}}[\bar{x},\bar{p}] = S_{\text{int}}[x,p]$ is a bit more involved and we present it below. Using the symmetries of $G(x,y,t)$ reported in equations (106) and (107), we can write the time-reversed action in the form

$$\begin{aligned} S_{\text{int}}[\bar{x}(t), \bar{p}(t)] = & \frac{V_{\text{eff}}(x_{\infty})}{T} \\ & + \frac{1}{T}\int dt dt'\, \theta(t' - t)\dot{x}(t)[F(x(t), x(t'), t' - t) - \dot{x}(t') G(x(t), x(t'), t' - t)] \\ & + i\int dt dt'\, \theta(t' - t) p(t)[F(x(t), x(t'), t' - t) - \dot{x}(t') G(x(t), x(t'), t' - t)] \\ & - i\int dt dt'\, \theta(t - t') p(t) G(x(t), x(t'), t - t')\dot{x}(t') \\ & + \frac{T}{2}\int dt dt'\, p(t) G(x(t), x(t'), t - t') p(t'). \end{aligned} \tag{112}$$

We note that the last term in the time-reversed action coincides with the last term in the original action (109). From the relations given in equations (103) and (104), one obtains

$$-\frac{d'}{dt}\psi(x(t), x(t'), t' - t) = F(x(t), x(t'), t' - t) - \dot{x}(t') G(x(t), x(t'), t' - t), \tag{113}$$

$$\frac{d'}{dt}\psi(x(t), x(t'), t - t') = F(x(t), x(t'), t - t') + \dot{x}(t') G(x(t), x(t'), t - t'). \tag{114}$$

Accordingly, the time-reversed action in equation (112) can be written as

$$\begin{aligned} S_{\text{int}}[\bar{x}(t), \bar{p}(t)] = & \frac{V_{\text{eff}}(x_{\infty})}{T} - \frac{1}{T}\int dt\, \dot{x}(t)\int_t^{\infty} dt' \frac{d'}{dt}[\psi(x(t), x(t'), t' - t)] \\ & - i\int dt\, p(t)\int_t^{\infty} dt' \frac{d'}{dt}[\psi(x(t), x(t'), t' - t)] \\ & - i\int dt\, p(t)\int_{-\infty}^{t} dt' \frac{d'}{dt}[\psi(x(t), x(t'), t - t')] \\ & + i\int dt dt'\, \theta(t - t') p(t) F(x(t), x(t'), t - t') \\ & + \frac{T}{2}\int dt dt'\, p(t) G(x(t), x(t'), t - t') p(t'). \end{aligned} \tag{115}$$

We notice that $\psi(x,y,t) \xrightarrow[t\to\infty]{} 0$ and that the two integrals in the second and the third line of equation (115) cancel each other out. Moreover, the last two terms coincide with the last two terms of the forward-time action in equation (109). Hence, in order to prove time-reversal symmetry, we have to show that the first term in equation (109) is equal to the two terms in the first line in equation (115). We note that, due to equation (105),

$$\begin{aligned}
&\frac{V_{\rm eff}(x_\infty)}{T} - \frac{1}{T}\int \mathrm{d}t\dot{x}(t)\int_t^\infty \mathrm{d}t'\frac{\mathrm{d}}{\mathrm{d}t'}\left[\psi(x(t),x(t'),t'-t)\right] \\
&\quad = \frac{V_{\rm eff}(x_\infty)}{T} + \frac{1}{T}\int \mathrm{d}t\dot{x}(t)\,\psi(x(t),x(t),0) \\
&\quad = \frac{V_{\rm eff}(x_\infty)}{T} - \frac{1}{T}\int \mathrm{d}t\frac{\mathrm{d}x}{\mathrm{d}t}\frac{\mathrm{d}V_{\rm eff}(x(t))}{\mathrm{d}x(t)} \\
&\quad = \frac{V_{\rm eff}(x_\infty)}{T} - \frac{1}{T}\int_{x_{-\infty}}^{x_\infty}\mathrm{d}x\frac{\mathrm{d}V_{\rm eff}(x)}{\mathrm{d}x} = \frac{V_{\rm eff}(x_{-\infty})}{T}
\end{aligned} \tag{116}$$

which concludes the proof of time-reversal symmetry of the action of the process.

Appendix D. Perturbative expansion

In this appendix, we solve the dynamics given by equations (14) and (15) in the case of a one-dimensional system with a point-like particle, see equation (9). First, we state the formal solutions of the dynamics within the perturbative expansion (52) and (53), and report properties of the Ornstein–Uhlenbeck process relevant for further calculations. Then, in appendix D.1, we demonstrate that evaluating the lowest-order correction to the average particle position obtained from the equations of motion yields the same result as the one obtained from the Gibbs–Boltzmann distribution, reported in equation (32). Finally, we derive the lowest-order correction to the connected two-point function, reported in equations (57)–(59).

Applying the expansion in powers of λ to ϕ and X, see equations (52) and (53), respectively, to the dynamics (14) and (15), and solving it term-by-term for the field configuration yields

$$\phi^{(0)}(x,t) = \int_{-\infty}^t \mathrm{d}t'\int_0^\infty \mathrm{d}x'\,\frac{1}{D}R_\phi^D(x,x',t-t')\,\xi(x',t'), \tag{117}$$

$$\lambda\phi^{(1)}(x,t) = \lambda\int_{-\infty}^t \mathrm{d}t'\int_0^\infty \mathrm{d}x'\,R_\phi^D(x,x',t-t')\,V\left(x'-X^{(0)}(t')\right), \tag{118}$$

where the R_ϕ^D is defined in equations (37) and (38). Solving for the particle position and using equation (20) renders

$$X^{(0)}(t) = X_0 + \gamma_0^{-1}\int_{-\infty}^t \mathrm{d}t'\,e^{-\omega_0(t-t')}\eta(t') = X_0 + \tilde{X}(t), \tag{119}$$

$$\lambda X^{(1)}(t) = \gamma_0^{-1}\int_{-\infty}^t \mathrm{d}t'\,e^{-\omega_0(t-t')}\Xi\left(X^{(0)}(t'),t'\right), \tag{120}$$

$$\begin{aligned}
\lambda^2 X^{(2)}(t) &= \gamma_0^{-1}\int_{-\infty}^t \mathrm{d}t'\,e^{-\omega_0(t-t')}\int_{-\infty}^{t'}\mathrm{d}t''F\left(X^{(0)}(t'),X^{(0)}(t''),t'-t''\right) \\
&\quad + \gamma_0^{-1}\int_{-\infty}^t \mathrm{d}t'\,e^{-\omega_0(t-t')}\lambda X^{(1)}(t')\,\partial_X\Xi\left(X^{(0)}(t'),t'\right),
\end{aligned} \tag{121}$$

where ω_0 is defined below equation (56). While deriving $X^{(1)}$, we used the expressions of $\phi^{(0)}$ and Ξ in equations (117) and (100), respectively. Note that in equation (119) we introduced $\tilde{X}(t)$, which is the Ornstein–Uhlenbeck process characterized by the transition probability

$$\mathcal{P}(x_1,t_1|x_2,t_2) = \frac{1}{\sqrt{2\pi\ell_T^2\left(1-e^{-2\omega_0(t_1-t_2)}\right)}}\exp\left\{-\frac{1}{2}\frac{\left(x_1-x_2e^{-\omega_0(t_1-t_2)}\right)^2}{\ell_T^2\left(1-e^{-2\omega_0(t_1-t_2)}\right)}\right\}, \tag{122}$$

where ℓ_T is the thermal lengthscale defined below equation (19). For the sake of further derivations, using equation (122), we evaluate the following quantities

$$\langle e^{ik_1X^{(0)}(t_1)+ik_2X^{(0)}(t_2)}\rangle = \exp\left[i(k_1+k_2)X_0 - \frac{\ell_T^2}{2}\left(k_1^2+2k_1k_2e^{-\omega_0|t_1-t_2|}+k_2^2\right)\right], \tag{123}$$

and

$$\langle e^{ik_1X^{(0)}(t_1)+ik_2X^{(0)}(t_2)}\tilde{X}(t_3)\rangle = i\ell_T^2\left(k_1e^{-\omega_0|t_1-t_3|}+k_2e^{-\omega_0|t_2-t_3|}\right) \times \exp\left[i(k_1+k_2)X_0 - \frac{\ell_T^2}{2}\left(k_1^2+2k_1k_2e^{-\omega_0|t_1-t_2|}+k_2^2\right)\right]. \tag{124}$$

Additionally, we note that for a point-like particle, equation (36) renders

$$F(x,y,t) = -i\lambda^2D\int\frac{\mathrm{d}k}{2\pi}ke^{-D\left(k^2+r\right)t}\left[e^{-ik(x-y)}-e^{-ik(x+y)}\right], \tag{125}$$

while

$$G(x,y,t) = \lambda^2\int\frac{\mathrm{d}k}{2\pi}\frac{k^2}{k^2+r}e^{-D\left(k^2+r\right)|t|}\left[e^{-ik(x-y)}+e^{-ik(x+y)}\right], \tag{126}$$

which follows from equation (40), where in both cases we omit the indication of the component of the vector, as we are considering the case $d=1$. We conclude the preliminary remarks of the appendix by recalling that the equations of motion (14) and (15) are invariant under the transformation (16). Hence, $\langle X\rangle$ and $\langle X^2\rangle$ are even functions of λ.

D.1. The average position

The lowest-order correction to the average position of the particle is given by

$$\lambda^2\langle X^{(2)}(t)\rangle = \frac{1}{\gamma_0}\int_{-\infty}^{t}\mathrm{d}t'\,e^{-\omega_0\left(t-t'\right)}\int_{-\infty}^{t'}\mathrm{d}t''\left\langle F\left(X^{(0)}(t'),X^{(0)}(t''),t'-t''\right)\right\rangle + \frac{T}{\gamma_0^2}\int_{-\infty}^{t}\mathrm{d}t'\,e^{-\omega_0\left(t-t'\right)}\int_{-\infty}^{t'}\mathrm{d}t''\,e^{-\omega_0\left(t'-t''\right)}\left\langle\partial_{X^{(0)}(t')}G\left(X^{(0)}(t'),X^{(0)}(t''),t'-t''\right)\right\rangle, \tag{127}$$

where we used equation (39) for the average of the field-induced noise. Making use of equations (123) and (125) renders the first term in the sum on the right-hand side of equation (127), i.e.

$$\left\langle F\left(X^{(0)}(t'),X^{(0)}(t''),t'-t''\right)\right\rangle = \lambda^2D\int\frac{\mathrm{d}k}{2\pi}e^{-D\left(k^2+r\right)\left(t'-t''\right)-\ell_T^2k^2\left(1+e^{-\omega_0\left(t'-t''\right)}\right)}k\sin(2X_0k). \tag{128}$$

In a similar way, from equations (126) and (123), we obtain

$$\left\langle\partial_{X^{(0)}(t')}G\left(X^{(0)}(t'),X^{(0)}(t''),t'-t''\right)\right\rangle = -\lambda^2\int\frac{\mathrm{d}k}{2\pi}e^{-D\left(k^2+r\right)|t'-t''|-\ell_T^2k^2\left(1+e^{-\omega_0|t'-t''|}\right)}\frac{k^3\sin(2X_0k)}{k^2+r}. \tag{129}$$

Note that in equations (128) and (129), we kept only the terms of the integrand which are even functions of k. In fact, according to equation (123), the translationally-invariant terms in equations (125) and (126) will give rise to additional terms which are odd functions of k, and which vanish after integrating over the wavevector. Summing equations (128) and (129) yields

$$\langle\lambda^2X^{(2)}(t)\rangle = \frac{\lambda^2}{\kappa}\int\frac{\mathrm{d}k}{2\pi}\frac{k\sin(2X_0k)}{k^2+r}\int_0^\infty\mathrm{d}u\left[D\left(k^2+r\right)-\ell_T^2k^2\omega_0e^{-\omega_0u}\right]e^{-D\left(k^2+r\right)u-\ell_T^2k^2\left(1+e^{-\omega_0u}\right)}. \tag{130}$$

Note that the integrand of this function can actually be written as a total derivative, i.e.

$$\left[D\left(k^2+r\right)-\ell_T^2k^2\omega_0e^{-\omega_0u}\right]e^{-D\left(k^2+r\right)u-\ell_T^2k^2\left(1+e^{-\omega_0u}\right)} \\ =-\frac{\mathrm{d}}{\mathrm{d}u}\left[e^{-D\left(k^2+r\right)u-\ell_T^2k^2\left(1+e^{-\omega_0u}\right)}\right]. \tag{131}$$

Using this fact in equation (130) makes the integral over u straightforward and leads to

$$\begin{aligned}\lambda^2\langle X^{(2)}(t)\rangle &= \frac{\lambda^2}{\kappa}\int\frac{\mathrm{d}k}{2\pi}\frac{e^{-2\ell_T^2k^2}k\sin(2X_0k)}{k^2+r}\\ &=\frac{\lambda^2}{4\kappa}e^{-\frac{2X_0}{\xi}+\frac{2\ell_T^2}{\xi^2}}\left[\mathrm{Erfc}\left(\frac{\sqrt{2}\ell_T}{\xi}-\frac{X_0}{\sqrt{2}\ell_T}\right)-\mathrm{Erfc}\left(\frac{\sqrt{2}\ell_T}{\xi}+\frac{X_0}{\sqrt{2}\ell_T}\right)\right]\\ &\xrightarrow[X_0/\ell_T\to\infty]{}\frac{\lambda^2}{2\kappa}e^{-\frac{2X_0}{\xi}+\frac{2\ell_T^2}{\xi^2}}\end{aligned} \tag{132}$$

where $\mathrm{Erfc}(x)=2/\sqrt{\pi}\int_x^\infty \mathrm{d}u\, e^{-u^2}$ is the complementary error function. The calculation recovers the result obtained using the Gibbs–Boltzmann distribution reported in equation (31).

D.2. The correlation function

The lowest-order correction to the particle two-point correlation function is

$$\lambda^2C^{(2)}(t)=\lambda^2\langle X^{(2)}(t_1)X^{(0)}(t_2)+X^{(1)}(t_1)X^{(1)}(t_2)+X^{(0)}(t_1)X^{(2)}(t_2)\rangle, \tag{133}$$

where we denoted $t=t_2-t_1>0$ and used the stationarity of the process. Then, the correction to the connected two-point function is given by

$$\begin{aligned}\lambda^2C_c^{(2)}(t)&=\lambda^2C^{(2)}(t)-2X_0\lambda^2\langle X^{(2)}\rangle\\ &=\lambda^2\langle X^{(1)}(t_1)X^{(1)}(t_2)+\tilde{X}(t_1)X^{(2)}(t_2)+X^{(2)}(t_1)\tilde{X}(t_2)\rangle,\end{aligned} \tag{134}$$

where $\tilde{X}(t)$ is the Ornstein–Uhlenbeck process introduced in equation (119) characterized by the transition probability in equation (122). We now evaluate each term in the last line in equation (134), starting from the first one:

$$\begin{aligned}\lambda^2\left\langle X^{(1)}(t_1)X^{(1)}(t_2)\right\rangle &=\frac{1}{\gamma_0^2}\int_{-\infty}^{t_1}\mathrm{d}t_1'\,e^{-\omega_0\left(t_1-t_1'\right)}\int_{-\infty}^{t_2}\mathrm{d}t_2'\,e^{-\omega_0\left(t_2-t_2'\right)}\left\langle\Xi\left(X^{(0)}(t_1'),t_1'\right)\Xi\left(X^{(0)}(t_2'),t_2'\right)\right\rangle\\ &=\frac{T}{\gamma_0^2}\int_{-\infty}^{t_1}\mathrm{d}t_1'\,e^{-\omega_0\left(t_1-t_1'\right)}\int_{-\infty}^{t_2}\mathrm{d}t_2'\,e^{-\omega_0\left(t_2-t_2'\right)}\left\langle G\left(X^{(0)}(t_1'),X^{(0)}(t_2'),t_1'-t_2'\right)\right\rangle,\end{aligned} \tag{135}$$

where we used equations (119) and equation (39) for the correlation of the field-induced noise. Now, applying equation (123) to the expression for G in equation (126), we find

$$\begin{aligned}\left\langle G\left(X^{(0)}(t'),X^{(0)}(t''),t'-t''\right)\right\rangle &=\lambda^2\int\frac{\mathrm{d}k}{2\pi}e^{-D\left(k^2+r\right)|t'-t''|-\ell_T^2k^2\left(1-e^{-\omega_0|t'-t''|}\right)}\frac{k^2}{k^2+r}\\ &\quad+\lambda^2\int\frac{\mathrm{d}k}{2\pi}e^{-D\left(k^2+r\right)|t'-t''|-\ell_T^2k^2\left(1+e^{-\omega_0|t'-t''|}\right)}\frac{k^2\cos(2X_0k)}{k^2+r},\end{aligned} \tag{136}$$

where we kept only terms which are even functions of k. In order to simplify the notation, we introduce

$$F(u)=\int\frac{\mathrm{d}k}{2\pi}e^{-D\left(k^2+r\right)u}\frac{k^2}{k^2+r}\left[e^{-\ell_T^2k^2\left(1-e^{-\omega_0u}\right)}+e^{-\ell_T^2k^2\left(1+e^{-\omega_0u}\right)}\cos(2X_0k)\right] \tag{137}$$

which allows us to cast equation (135), after a suitable change of variables of integration, in the form

$$\lambda^2\left\langle X^{(1)}(t_1)X^{(1)}(t_2)\right\rangle=\frac{\lambda^2T}{\gamma_0^2}e^{-\omega_0t}\int_0^\infty\mathrm{d}t_1'\,e^{-\omega_0t_1'}\int_{-t}^\infty\mathrm{d}t_2'\,e^{-\omega_0t_2'}F(|t_1'-t_2'|). \tag{138}$$

A direct calculation shows that

$$\int_0^\infty \mathrm{d}t_1' \, e^{-\omega_0 t_1'} \int_{-t}^\infty \mathrm{d}t_2' \, e^{-\omega_0 t_2'} F\left(|t_1' - t_2'|\right)$$
$$= \frac{1}{2\omega_0}\left[\int_0^\infty \mathrm{d}u \, e^{-\omega_0 u} F(u) + \int_0^t \mathrm{d}u \, e^{\omega_0 u} F(u) + e^{2\omega_0 t}\int_t^\infty \mathrm{d}u \, e^{-\omega_0 u} F(u)\right]. \tag{139}$$

This leads to

$$\lambda^2 \left\langle X^{(1)}(t_1) X^{(1)}(t_2)\right\rangle = \frac{\lambda^2 \ell_T^2}{2\kappa}\omega_0 \left[\int_0^\infty \mathrm{d}u \, e^{-\omega_0 (u+t)} F(u) + \int_0^t \mathrm{d}u \, e^{-\omega_0 (t-u)} F(u) + \int_t^\infty \mathrm{d}u \, e^{\omega_0 (t-u)} F(u)\right]. \tag{140}$$

We now turn our attention to the second term in the last line of equation (134), i.e.

$$\lambda^2 \left\langle \tilde{X}(t_1) X^{(2)}(t_2)\right\rangle = \frac{1}{\gamma_0^2}\int_{-\infty}^{t_2} \mathrm{d}t_2' \int_{-\infty}^{t_2} \mathrm{d}t_2'' \, e^{-\omega_0 \left(t_2 - t_2''\right)} \left\langle \tilde{X}(t_1) \partial_{X^{(0)}(t_2')} \Xi\left(X^{(0)}(t_2'), t_2'\right) \Xi\left(X^{(0)}(t_2''), t_2''\right)\right\rangle$$
$$+ \frac{1}{\gamma_0}\int_{-\infty}^{t_2} \mathrm{d}t_2' \, e^{-\omega_0 \left(t_2 - t_2'\right)} \int_{-\infty}^{t_2} \mathrm{d}t_2'' \left\langle \tilde{X}(t_1) F\left(X^{(0)}(t_2'), X^{(0)}(t_2''), t_2' - t_2''\right)\right\rangle, \tag{141}$$

where we used the expression for $\lambda^2 X^{(2)}$ in equation (121). We evaluate the average in the first term of equation (141) using the definition of G in equations (39) and (126), and the property of the Ornstein–Uhlenbeck process in equation (124), concluding that

$$\left\langle \tilde{X}(t_1) \partial_{X^{(0)}(t_2')} \Xi\left(X^{(0)}(t_2'), t_2'\right) \Xi\left(X^{(0)}(t_2''), t_2''\right)\right\rangle$$
$$= -i\lambda^2 T \int \frac{\mathrm{d}k}{2\pi} \frac{e^{-D\left(k^2+r\right)\left(t_2' - t_2''\right)}}{k^2 + r} k^3 \left\langle \tilde{X}(t_1) e^{-ik\left(X^{(0)}(t_2') - X^{(0)}(t_2'')\right)}\right\rangle$$
$$- i\lambda^2 T \int \frac{\mathrm{d}k}{2\pi} \frac{e^{-D\left(k^2+r\right)\left(t_2' - t_2''\right)}}{k^2 + r} k^3 \left\langle \tilde{X}(t_1) e^{-ik\left(X^{(0)}(t_2') + X^{(0)}(t_2'')\right)}\right\rangle,$$
$$= -\lambda^2 T \ell_T^2 \int \frac{\mathrm{d}k}{2\pi} e^{-D(k^2+r)(t_2' - t_2'') - \ell_T^2 k^2\left(1 - e^{-\omega_0 (t_2' - t_2'')}\right)} \frac{k^4}{k^2 + r}\left(e^{-\omega_0 |t_1 - t_2'|} - e^{-\omega_0 |t_1 - t_2''|}\right)$$
$$- \lambda^2 T \ell_T^2 \int \frac{\mathrm{d}k}{2\pi} e^{-D(k^2+r)(t_2' - t_2'') - \ell_T^2 k^2\left(1 + e^{-\omega_0 (t_2' - t_2'')}\right)} \frac{k^4 \cos(2X_0 k)}{k^2 + r}\left(e^{-\omega_0 |t_1 - t_2'|} + e^{-\omega_0 |t_1 - t_2''|}\right). \tag{142}$$

Similarly, we calculate the average in the second term in equation (141), utilizing equations (124) and (125). This yields

$$\left\langle \tilde{X}(t_1) F\left(X^{(0)}(t_2'), X^{(0)}(t_2''), t_2' - t_2''\right)\right\rangle$$
$$= -i\lambda^2 D \int \frac{\mathrm{d}k}{2\pi} e^{-D\left(k^2+r\right)\left(t_2' - t_2''\right)} k \left\langle \tilde{X}(t_1) e^{-ik\left(X^{(0)}(t_2') - X^{(0)}(t_2'')\right)}\right\rangle$$
$$+ i\lambda^2 D \int \frac{\mathrm{d}k}{2\pi} e^{-D\left(k^2+r\right)\left(t_2' - t_2''\right)} k \left\langle \tilde{X}(t_1) e^{-ik\left(X^{(0)}(t_2') + X^{(0)}(t_2'')\right)}\right\rangle$$
$$= -\lambda^2 D \ell_T^2 \int \frac{\mathrm{d}k}{2\pi} e^{-D\left(k^2+r\right)\left(t_2' - t_2''\right)} k^2 e^{-\ell_T^2 k^2\left(1 - e^{-\omega_0 (t_2' - t_2'')}\right)}\left(e^{-\omega_0 |t_1 - t_2'|} - e^{-\omega_0 |t_1 - t_2''|}\right)$$
$$+ \lambda^2 D \ell_T^2 \int \frac{\mathrm{d}k}{2\pi} e^{-D(k^2+r)(t_2' - t_2'') - \ell_T^2 k^2\left(1 + e^{-\omega_0 (t_2' - t_2'')}\right)} k^2 \cos(2X_0 k)\left(e^{-\omega_0 |t_1 - t_2'|} + e^{-\omega_0 |t_1 - t_2''|}\right). \tag{143}$$

Accordingly, using equations (142) and (143) in equation (141) renders

$$\lambda^2 \left\langle \tilde{X}(t_1) X^{(2)}(t_2)\right\rangle$$
$$= -\frac{\lambda^2 \ell_T^2}{2\pi \gamma_0}\int_{-\infty}^{t_2} \mathrm{d}t_2' \, e^{-\omega_0 \left(t_2 - t_2'\right)} \int_{-\infty}^{t_2'} \mathrm{d}t_2'' \left(e^{-\omega_0 |t_1 - t_2'|} - e^{-\omega_0 |t_1 - t_2''|}\right)$$
$$\times \int \frac{\mathrm{d}k \, k^2}{k^2 + r} e^{-D\left(k^2+r\right)\left(t_2' - t_2''\right) - \ell_T^2 k^2\left(1 - e^{-\omega_0 (t_2' - t_2'')}\right)} \left[D\left(k^2 + r\right) + \ell_T^2 k^2 \omega_0 e^{-\omega_0 \left(t_2' - t_2''\right)}\right]$$
$$+ \frac{\lambda^2 \ell_T^2}{2\pi \gamma_0}\int_{-\infty}^{t_2} \mathrm{d}t_2' \, e^{-\omega_0 \left(t_2 - t_2'\right)} \int_{-\infty}^{t_2'} \mathrm{d}t_2'' \left(e^{-\omega_0 |t_1 - t_2'|} + e^{-\omega_0 |t_1 - t_2''|}\right)$$
$$\times \int \frac{\mathrm{d}k \, k^2 \cos\left(2X_0 k\right)}{k^2 + r} e^{-D\left(k^2+r\right)\left(t_2' - t_2''\right) - \ell_T^2 k^2\left(1 + e^{-\omega_0 (t_2' - t_2'')}\right)} \left[D\left(k^2 + r\right) - \ell_T^2 k^2 \omega_0 e^{-\omega_0 \left(t_2' - t_2''\right)}\right]. \tag{144}$$

We decompose F defined in equation (137) into $F(u) = F^+(u) + F^-(u)$ with

$$F^+(u) = \int \frac{dk}{2\pi} e^{-D(k^2+r)u - \ell_T^2 k^2 \left(1-e^{-\omega_0 u}\right)} \frac{k^2}{k^2+r}, \tag{145}$$

$$F^-(u) = \int \frac{dk}{2\pi} e^{-D(k^2+r)u - \ell_T^2 k^2 \left(1+e^{-\omega_0 u}\right)} \frac{k^2 \cos(2X_0 k)}{k^2+r}, \tag{146}$$

and, similarly to equation (131), we note that

$$\left[D\left(k^2+r\right) + \ell_T^2 k^2 \omega_0 e^{-\omega_0 u}\right] e^{-D(k^2+r)u - \ell_T^2 k^2\left(1+e^{-\omega_0 u}\right)} = -\frac{d}{du}\left[e^{-D(k^2+r)u - \ell_T^2 k^2\left(1-e^{-\omega_0 u}\right)}\right]. \tag{147}$$

We can now change the variables of integration in equation (144) to $u = t_2' - t_2''$ and $v = t_1 - t_2'$, apply equations (131) and (147) along with the definitions of $F^+(u)$ and $F^-(u)$ in equations (145) and (146), respectively, to equation (144), and write

$$\begin{aligned}
\lambda^2 \left\langle \tilde{X}(t_1) X^{(2)}(t_2) \right\rangle &= \frac{\lambda^2 \ell_T^2}{\gamma_0} e^{-\omega_0 t} \int_{-t}^{\infty} dv\, e^{-\omega_0 v} \int_0^{\infty} du \left(e^{-\omega_0 |v|} - e^{-\omega_0 |v+u|}\right) \frac{dF^+(u)}{du} \\
&\quad - \frac{\lambda^2 \ell_T^2}{\gamma_0} e^{-\omega_0 t} \int_{-t}^{\infty} dv\, e^{-\omega_0 v} \int_0^{\infty} du \left(e^{-\omega_0 |v|} + e^{-\omega_0 |v+u|}\right) \frac{dF^-(u)}{du}, \\
&= \frac{\lambda^2 \ell_T^2}{\gamma_0} e^{-\omega_0 t} \left[2F^-(0) \int_{-t}^{\infty} dv\, e^{-\omega_0 (v+|v|)} + \int_{-t}^{\infty} dv\, e^{-\omega_0 v} \int_0^{\infty} du\, F(u) \frac{d}{du} e^{-\omega_0 |u+v|}\right].
\end{aligned} \tag{148}$$

Using the fact that

$$\begin{aligned}
&\int_{-t}^{\infty} dv\, e^{-\omega_0 v} \int_0^{\infty} du\, F(u) \frac{d}{du} e^{-\omega_0 |u+v|} \\
&\qquad = \frac{1}{2}\left\{\int_0^t du \left[2\omega_0 (t-u) - 1\right] e^{\omega_0 u} F(u) - e^{2\omega_0 t} \int_t^{\infty} du\, e^{-\omega_0 u} F(u)\right\},
\end{aligned} \tag{149}$$

one can cast equation (148) in the form

$$\begin{aligned}
\lambda^2 \left\langle \tilde{X}(t_1) X^{(2)}(t_2) \right\rangle &= \frac{\lambda^2 \ell_T^2}{\kappa} \left[e^{-\omega_0 t} F^-(0) (1 + 2\omega_0 t) + \omega_0 \int_0^t du\, \omega_0 (t-u) e^{-\omega_0 (t-u)} F(u)\right] \\
&\quad - \frac{\lambda^2 \ell_T^2}{2\kappa} \omega_0 \left[\int_0^t du\, e^{-\omega_0 (t-u)} F(u) + \int_t^{\infty} du\, e^{\omega_0 (t-u)} F(u)\right].
\end{aligned} \tag{150}$$

Finally, the calculation of the third term in equation (134) is very similar to that of the second one therein. Accordingly, we simply report the final expression

$$\lambda^2 \left\langle X^{(2)}(t_1) \tilde{X}(t_2) \right\rangle = \frac{\lambda^2 \ell_T^2}{2\kappa} \left[2e^{-\omega_0 t} F^-(0) - \omega_0 \int_0^{\infty} du\, e^{-\omega_0 (u+t)} F(u)\right]. \tag{151}$$

Summing the results of equations (140), (150) and (151) allows us to cast the expression for the connected part of the two-point function in equation (134) in the form

$$\lambda^2 C_c^{(2)}(t) = \frac{\lambda^2 \ell_T^2}{\kappa} \left[2e^{-\omega_0 t} F^-(0) (1 + \omega_0 t) + \omega_0 \int_0^t du\, \omega_0 (t-u) e^{-\omega_0 (t-u)} F(u)\right], \tag{152}$$

which is the expression provided in equation (59), which is expressed in terms of the dimensionless memory defined below in equation (156). For the sake of completeness, we note that a straightforward calculation renders the complete expression of $F^+(u)$ introduced in equation (145) in the form

$$F^{+}(u) = \frac{e^{-\frac{Du}{\xi^2}}}{\sqrt{4\pi\left(Du+\ell_T^2\left(1-e^{-\omega_0 u}\right)\right)}} - \frac{1}{2\xi}e^{\frac{\ell_T^2}{\xi^2}\left(1-e^{-\omega_0 u}\right)}\operatorname{Erfc}\left(\sqrt{\frac{Du}{\xi^2}+\frac{\ell_T^2}{\xi^2}\left(1-e^{-\omega_0 u}\right)}\right)$$
$$\xrightarrow[\xi\to\infty]{} \frac{1}{\sqrt{4\pi\left(Du+\ell_T^2\left(1-e^{-\omega_0 u}\right)\right)}} = F_c^{+}(u). \tag{153}$$

The limit $\xi\to\infty$ of the expression above is reported in the main text in equation (63). In addition, the complete expression of $F^{-}(u)$ can be obtained by performing the integral in equation (146):

$$F^{-}(u) = \frac{e^{-\left(\frac{Du}{\xi^2}+\frac{X_0^2}{Du+\ell_T^2\left(1+e^{-\omega_0 u}\right)}\right)}}{\sqrt{4\pi\left(Du+\ell_T^2\left(1+e^{-\omega_0 u}\right)\right)}}$$
$$-\frac{1}{4\xi}e^{-\frac{2X_0}{\xi}+\frac{\ell_T^2}{\xi^2}\left(1+e^{-\omega_0 u}\right)}\operatorname{Erfc}\left(\sqrt{\frac{Du}{\xi^2}+\frac{\ell_T^2}{\xi^2}\left(1+e^{-\omega_0 u}\right)}-\frac{X_0}{\sqrt{Du+\ell_T^2\left(1+e^{-\omega_0 u}\right)}}\right)$$
$$-\frac{1}{4\xi}e^{\frac{2X_0}{\xi}+\frac{\ell_T^2}{\xi^2}\left(1+e^{-\omega_0 u}\right)}\operatorname{Erfc}\left(\sqrt{\frac{Du}{\xi^2}+\frac{\ell_T^2}{\xi^2}\left(1+e^{-\omega_0 u}\right)}+\frac{X_0}{\sqrt{Du+\ell_T^2\left(1+e^{-\omega_0 u}\right)}}\right)$$
$$\xrightarrow[\xi\to\infty]{} \frac{e^{-\frac{X_0^2}{Du+\ell_T^2\left(1+e^{-\omega_0 u}\right)}}}{\sqrt{4\pi\left(Du+\ell_T^2\left(1+e^{-\omega_0 u}\right)\right)}} = F_c^{-}(u). \tag{154}$$

The limit $\xi\to\infty$ of the expression above is given in equation (64) of the main text. Finally, we note from equation (154) that

$$F^{-}(0) = \frac{e^{-\frac{X_0^2}{2\ell_T^2}}}{\sqrt{8\pi\ell_T^2}} - \frac{1}{4\xi}e^{-\frac{2X_0}{\xi}+\frac{2\ell_T^2}{\xi^2}}\operatorname{Erfc}\left(\frac{\sqrt{2}\ell_T}{\xi}-\frac{X_0}{\sqrt{2}\ell_T}\right)$$
$$-\frac{1}{4\xi}e^{\frac{2X_0}{\xi}+\frac{\ell_T^2}{\xi^2}\left(1+e^{-\omega_0 u}\right)}\operatorname{Erfc}\left(\frac{\sqrt{2}\ell_T}{\xi}+\frac{X_0}{\sqrt{2}\ell_T}\right)$$
$$\xrightarrow[X_0/\ell_T\to\infty]{} -\frac{1}{2\xi}e^{-\frac{2X_0}{\xi}+\frac{2\ell_T^2}{\xi^2}}. \tag{155}$$

Lastly, introducing the dimensionless memory $\mathcal{F}$ by

$$\frac{1}{\xi}\mathcal{F}(\omega_0 t) = F(t) \tag{156}$$

and combining the results in equations (152) and (155), renders the final expression of $\lambda^2 C_c^{(2)}(t)$ reported in equations (57)–(59) of the main text.

Appendix E. Power spectral density (PSD)

In order to derive the PSD reported in equation (72), we use

$$\int_{\mathbb{R}} \mathrm{d}t\, e^{i\omega t}\int_0^{\omega_0|t|}\mathrm{d}u\,(\omega_0|t|-u)\,e^{-(\omega_0|t|-u)}\mathcal{F}(u)$$
$$= \int_0^\infty \mathrm{d}t\, e^{i\omega t}\int_0^{\omega_0 t}\mathrm{d}u\,(\omega_0 t-u)\,e^{-(\omega_0 t-u)}\mathcal{F}(u) + \text{c.c.}$$
$$= \frac{1}{\omega_0}\int_0^\infty \mathrm{d}u\, e^{i\frac{\omega}{\omega_0}u}\mathcal{F}(u)\int_u^\infty \mathrm{d}t\, e^{-(t-u)\left(1-i\frac{\omega}{\omega_0}\right)}(t-u) + \text{c.c.}$$
$$= \frac{1}{\omega_0}\frac{\omega_0^2}{(\omega_0-i\omega)^2}\int_0^\infty \mathrm{d}u\, e^{i\frac{\omega}{\omega_0}u}\mathcal{F}(u) + \text{c.c.}, \tag{157}$$

where *c.c.* denotes the complex conjugate. Then, using the properties of trigonometric functions, yields

$$\frac{\omega_0^2}{(\omega_0-i\omega)^2}e^{i\frac{\omega}{\omega_0}u} + \text{c.c.} = \frac{2\omega_0^4}{\left(\omega_0^2+\omega^2\right)^2}\left[\left(1-\frac{\omega^2}{\omega_0^2}\right)\cos\left(u\frac{\omega}{\omega_0}\right) - 2\frac{\omega}{\omega_0}\sin\left(u\frac{\omega}{\omega_0}\right)\right], \tag{158}$$

which proves the form of the PSD given in equation (72).

Appendix F. Bulk memory at higher dimensions

In this appendix, we derive the lowest order correction to the two-point function (54) in the case of the bulk system ($X_0 \to \infty$) for any d. It turns out that in such a case, the Casimir contribution defined in equation (58) vanishes, and $\lambda^2 C_c^{(2)}(t)$ is equal to the memory-induced contribution. Further, we focus on the critical case ($\xi \to \infty$) in which $\lambda^2 C_{c,\mathrm{memo}}^{(2)}(t)$ develops a power-law tail, i.e. it decays $\sim t^{-d/2}$.

We note that in the absence of the wall, the system recovers translational invariance, and it is convenient to express the fluctuating field in terms of its Fourier transform

$$\phi(\mathbf{x},t) = \int \frac{\mathrm{d}^d\mathbf{k}}{(2\pi)^d} e^{i\mathbf{k}\cdot\mathbf{x}} \tilde{\phi}_{\mathbf{k}}(t), \tag{159}$$

$$\tilde{\phi}_{\mathbf{k}}(t) = \int \mathrm{d}^d\mathbf{x}\, e^{-i\mathbf{k}\cdot\mathbf{x}} \phi(\mathbf{x},t). \tag{160}$$

In the Fourier-space, the equations of motion for the field (14) and for the particle (15) take the form

$$\left[\partial_t + D\left(r+k^2\right)\right]\tilde{\phi}_{\mathbf{k}}(t) = \lambda D e^{-i\mathbf{k}\cdot\mathbf{X}(t)} \tilde{V}_{\mathbf{k}} + \tilde{\zeta}_{\mathbf{k}}(t), \tag{161}$$

$$\gamma_0 \dot{\mathbf{X}}(t) + \kappa \mathbf{X}(t) = i\lambda \int \frac{\mathrm{d}^d\mathbf{k}}{(2\pi)^d} \mathbf{k}\tilde{\phi}_{\mathbf{k}}(\mathbf{x}) e^{i\mathbf{k}\cdot\mathbf{X}(t)} \tilde{V}_{-\mathbf{k}} + \boldsymbol{\eta}(t). \tag{162}$$

Utilizing the perturbative expansion in equation (52) and equation (53), and using the calculational framework presented in appendix D, one can evaluate the lowest-order correction to the two-point function (54) via a calculation analogous to the one sketched in appendix D.2. This renders

$$\lambda^2 C_c^{(2)}(t) = \frac{\lambda^2 \ell_T^2}{\kappa}\omega_0 \int_0^t \mathrm{d}u\, \omega_0 (t-u)\, e^{-\omega_0(t-u)} \int \frac{\mathrm{d}^d\mathbf{k}}{(2\pi)^d} \frac{k^2}{k^2+r} e^{-D\left(k^2+r\right)u - k^2\ell_T^2\left(1-e^{-\omega_0 u}\right)}. \tag{163}$$

Note the lack of the Casimir term in the expression above. We note that the result above is tantamount to putting $F^-(u)$ (see equation (146)) to 0, and

$$F^+(u) = \int \frac{\mathrm{d}^d\mathbf{k}}{(2\pi)^d} \frac{k^2}{k^2+r} e^{-D\left(k^2+r\right)u - \ell_T^2 k^2\left(1-e^{-\omega_0 u}\right)}, \tag{164}$$

where $F^+(u)$ is given by equation (145). At the critical point ($r=0$), a straightforward Gaussian integration yields

$$\lambda^2 C_c^{(2)}(t) = \frac{\lambda^2 \ell_T^2}{\kappa}\omega_0 \int_0^t \mathrm{d}u\, \omega_0 (t-u)\, e^{-\omega_0(t-u)} \left[4\pi\left(Du + \ell_T^2\left(1-e^{-\omega_0 u}\right)\right)\right]^{-d/2}. \tag{165}$$

Hence, for $\omega_0 t \gg 1$, it is characterized asymptotically by the behavior

$$\lambda^2 C_c^{(2)}(t) \sim \frac{\lambda^2 \ell_T^2}{\kappa}(4\pi D t)^{-d/2}. \tag{166}$$

It is worth noting that in the case of the model B dynamics in the bulk [12], this correction followed a power law of the form $\sim t^{-d/4}$. This can be understood as a consequence of the scaling following from the dynamical critical exponent, i.e. that the typical timescale in the system τ_ϕ scales with the correlation length as $\tau_\phi \sim \xi^z$ with $z = 2, 4$ for model A and model B, respectively.

ORCID iDs

Marcin Piotr Pruszczyk 0000-0003-2344-3333
Andrea Gambassi 0000-0003-3450-6125

References

[1] Einstein A 1905 *Ann. Phys.* **322** 549
[2] von Smoluchowski M 1906 *Ann. Phys.* **326** 756
[3] Coffey W T, Kalmykov Y P and Waldron J T 2004 *The Langevin Equation* 2nd edn (World Scientific) (https://doi.org/10.1142/5343)

[4] Kubo R, Toda M and Hashitsume N 2012 *Statistical Physics II: Nonequilibrium Statistical Mechanics* 2nd edn (*Springer Series in Solid-State Sciences*) (Springer) (https://doi.org/10.1007/978-3-642-58244-8)
[5] Franosch T, Grimm M, Belushkin M, Mor F M, Foffi G, Forró L and Jeney S 2011 *Nature* **478** 85–88
[6] Gomez-Solano J R and Bechinger C 2015 *New J. Phys.* **17** 103032
[7] Ginot F and Bechinger C 2025 *Nat. Commun.* **16** 10114
[8] Mason T G and Weitz D A 1995 *Phys. Rev. Lett.* **74** 1250
[9] Wirtz D 2009 *Annu. Rev. Biophys.* **38** 301
[10] Daldrop J O, Kowalik B G and Netz R R 2017 *Phys. Rev. X* **7** 041065
[11] Müller B, Berner J, Bechinger C and Krüger M 2020 *New J. Phys.* **22** 023014
[12] Basu U, Démery V and Gambassi A 2022 *SciPost Phys.* **13** 078
[13] Hohenberg P C and Halperin B I 1977 *Rev. Mod. Phys.* **49** 435
[14] Démery V and Dean D S 2010 *Phys. Rev. Lett.* **104** 080601
[15] Démery V and Dean D S 2010 *Eur. Phys. J. E* **32** 377
[16] Démery V and Dean D S 2011 *Phys. Rev. E* **84** 011148
[17] Dean D S and Démery V 2011 *J. Phys.: Condens. Matter* **23** 234114
[18] Démery V and Fodor É 2019 *J. Stat. Mech.* **2019** 033202
[19] Démery V, Bénichou O and Jacquin H 2014 *New J. Phys.* **16** 053032
[20] Gross M 2021 *J. Stat. Mech.* **2021** 063209
[21] Venturelli D and Gross M 2022 *J. Stat. Mech.* **2022** 123210
[22] Venturelli D, Ferraro F and Gambassi A 2022 *Phys. Rev. E* **105** 054125
[23] Venturelli D and Gambassi A 2022 *Phys. Rev. E* **106** 044112
[24] Venturelli D, Loos S A M, Walter B, Roldán É and Gambassi A 2024 *Europhys. Lett.* **146** 27001
[25] Démery V and Gambassi A 2023 *Phys. Rev. E* **108** 044604
[26] Venturelli D and Gambassi A 2023 *New J. Phys.* **25** 093025
[27] Pruszczyk M P, Venturelli D and Gambassi A 2025 *J. Stat. Mech.* **2025** 113202
[28] Huang K 2000 *Statistical Mechanics* (Wiley) (available at: https://books.google.fr/books?id = jbNTewAACAAJ)
[29] Täuber U C 2014 *Critical Dynamics: A Field Theory Approach to Equilibrium and Non-Equilibrium Scaling Behavior* (Cambridge University Press) (https://doi.org/10.1017/CBO9781139046213)
[30] Kardar M and Golestanian R 1999 *Rev. Mod. Phys.* **71** 1233
[31] Krech M 1994 *The Casimir Effect in Critical Systems* (World Scientific) (https://doi.org/10.1142/2434)
[32] Brankov J G, Danchev D M and Tonchev N S 2000 *Theory of Critical Phenomena in Finite-Size Systems* (World Scientific) (https://doi.org/10.1142/4146)
[33] Gambassi A 2009 *J. Phys.: Conf. Ser.* **161** 012037
[34] Gambassi A and Dietrich S 2024 *Soft Matter* **20** 3212
[35] Casimir H B 1948 *Proc. K. Ned. Akad. Wet.* **51** 793
[36] Fisher M E and De Gennes P G 1978 *C. R. Acad. Sci., Paris B* **287** 207
[37] Evans R and Stecki J 1994 *Phys. Rev. B* **49** 8842
[38] Dantchev D and Krech M 2004 *Phys. Rev. E* **69** 046119
[39] Martin P A and Zagrebnov V A 2006 *Europhys. Lett.* **73** 15–20
[40] Napiórkowski M, Jakubczyk P and Nowak K 2013 *J. Stat. Mech.* **2013** 06015
[41] Krech M and Dietrich S 1992 *Phys. Rev. A* **46** 1886
[42] Vasilyev O A and Dietrich S 2013 *Europhys. Lett.* **104** 60002
[43] Garcia R and Chan M H W 1999 *Phys. Rev. Lett.* **83** 1187
[44] Garcia R and Chan M H W 2002 *Phys. Rev. Lett.* **88** 086101
[45] Fukuto M, Yano Y F and Pershan P S 2005 *Phys. Rev. Lett.* **94** 135702
[46] Ganshin A, Scheidemantel S, Garcia R and Chan M H W 2006 *Phys. Rev. Lett.* **97** 075301
[47] Rafaï S, Bonn D and Meunier J 2007 *Physica A* **386** 31
[48] Hertlein C, Helden L, Gambassi A, Dietrich S and Bechinger C 2008 *Nature* **451** 172
[49] Ortiz de Zárate J M and Sengers J 2006 *Hydrodynamic Fluctuations in Fluids and Fluid Mixtures* (Elsevier) (https://doi.org/10.1016/B978-0-444-51515-5.X5000-5)
[50] Gambassi A 2008 *Eur. Phys. J. B* **64** 379
[51] Rohwer C M, Solon A, Kardar M and Krüger M 2018 *Phys. Rev. E* **97** 032125
[52] Gross M, Rohwer C M and Dietrich S 2019 *Phys. Rev. E* **100** 012114
[53] Gambassi A and Dietrich S 2006 *J. Stat. Phys.* **123** 929
[54] Cattuto C, Brito R, Marini Bettolo Marconi U, Nori F and Soto R 2006 *Phys. Rev. Lett.* **96** 178001
[55] Brito R, Marini Bettolo Marconi U and Soto R 2007 *Phys. Rev. E* **76** 011113
[56] Brito R, Soto R and Marini Bettolo Marconi U 2007 *Granul. Matter* **10** 29–36
[57] Kirkpatrick T R, Ortiz de Zárate J M and Sengers J V 2015 *Phys. Rev. Lett.* **115** 035901
[58] Fava G, Gambassi A and Ginelli F 2024 *Phys. Rev. Lett.* **133** 148301
[59] Furukawa A, Gambassi A, Dietrich S and Tanaka H 2013 *Phys. Rev. Lett.* **111** 055701
[60] Martínez I A, Devailly C, Petrosyan A and Ciliberto S 2017 *Entropy* **19** 77
[61] Eisenriegler E and Ritschel U 1995 *Phys. Rev. B* **51** 13717
[62] Binder K 1983 Critical behaviour at surfaces *Phase Transitions and Critical Phenomena* 8 and (Academic) pp 1–144
[63] Diehl H W 1986 Field-theoretic approach to critical behaviour at surfaces *Phase Transitions and Critical Phenomena* 10 and (Academic) pp 75–267
[64] Napiórkowski M and Piasecki J 2011 *Phys. Rev. E* **84** 061105
[65] Schmidt F, Callegari A, Daddi-Moussa-Ider A, Munkhbat B, Verre R, Shegai T, Käll M, Löwen H, Gambassi A and Volpe G 2023 *Nat. Phys.* **19** 271
[66] Dantchev D and Dietrich S 2023 *Phys. Rep.* **1005** 1
[67] Zinn-Justin J 2007 *Phase Transitions and Renormalization Group* (Oxford University Press) (https://doi.org/10.1093/acprof:oso/9780199227198.001.0001)

[68] Kawasaki K 1994 *Physica A* **208** 35
[69] Dean D S 1996 *J. Phys. A* **29** L613
[70] Jeney S, Lukić B, Kraus J A, Franosch T and Forró L 2008 *Phys. Rev. Lett.* **100** 240604
[71] Diehl H W and Janssen H K 1992 *Phys. Rev. A* **45** 7145
[72] Gross M 2018 *J. Stat. Mech.* **2018** 033212
[73] Bartolo D, Ajdari A, Fournier J B and Golestanian R 2002 *Phys. Rev. Lett.* **89** 230601
[74] Gross M, Gambassi A and Dietrich S 2021 *Phys. Rev. E* **103** 062118
[75] Napiórkowski M and Pruszczyk M 2022 *J. Stat. Mech.* **2022** 073104
[76] Burkhardt T W and Eisenriegler E 1995 *Phys. Rev. Lett.* **74** 3189
[77] Hanke A, Schlesener F, Eisenriegler E and Dietrich S 1998 *Phys. Rev. Lett.* **81** 1885
[78] Schlesener F, Hanke A and Dietrich S 2003 *J. Stat. Phys.* **110** 981
[79] Fournier J B 2021 arXiv:2112.14184
[80] Furst E M and Squires T M 2017 *Microrheology* (Oxford University Press) (https://doi.org/10.1093/oso/9780199655205.001.0001)
[81] Maruyama G 1955 *Rend. Circ. Mat. Palermo* **4** 48–90
[82] Martin P C, Siggia E D and Rose H A 1973 *Phys. Rev. A* **8** 423
[83] De Dominicis C 1976 *J. Phys. Colloq.* **37** C1–247–C1–253
[84] Janssen H K 1976 *Z. Phys. B* **23** 377
[85] Aron C, Biroli G and Cugliandolo L F 2010 *J. Stat. Mech.* **2010** 11018